Available online at www.sciencedirect.com
ScienceDirect
Ore Geology Reviews 31 (2007) 337–359
ORE GEOLOGY REVIEWS
www.elsevier.com/locate/oregeorev

Geologic, fluid inclusion and isotopic characteristics of the Jinding Zn–Pb deposit, western Yunnan, South China: A review

Chunji Xue [a,*], Rong Zeng [b], Shuwen Liu [b], Guoxiang Chi [c], Hairuo Qing [c], Yuchuan Chen [d], Jianmin Yang [d], Denghong Wang [d]

[a] *State Key Laboratory of Geological Processes and Mineral Resources, China University of Geosciences, Beijing 100083, China*
[b] *Faculty of Earth Sciences and Land Resources, Chang'an University, Xi'an 710054, China*
[c] *Department of Geology, University of Regina, Regina, Saskatchewan, Canada S42 0A2*
[d] *Chinese Academy of Geological Sciences, Beijing, 100037, China*

Received 26 February 2003; accepted 2 April 2005
Available online 30 June 2006

Abstract

With a reserve of ~200 Mt ore grading 6.08% Zn and 1.29% Pb (i.e., a metal reserve of ~15 Mt) hosted in Cretaceous and Tertiary terrestrial rocks, the Jinding deposit is the largest Zn–Pb deposit in China, and also the youngest sediment-hosted super giant Zn–Pb deposit in the world. The deposit mainly occurs in the Jinding dome structure as tabular orebodies within breccia-bearing sandstones of the Palaeocene Yunlong Formation (autochthonous) and in the overlying sandstones of the Early Cretaceous Jingxing Formation (allochthonous). The deposit is not stratiform and no exhalative sedimentary rocks have been observed. The occurrence of the orebodies, presence of hangingwall alteration, and replacement and open-space filling textures all indicate an epigenetic origin. Formation of the Jinding Zn–Pb deposit is related to a period of major continental crust movement during the collision of the Indian and Eurasian Plates. The westward thrusts and dome structure were successively developed in the Palaeocene sedimentary rocks in the ore district, and Zn–Pb mineralisation appears to have taken place in the early stage of the doming processes.

The study of fluid inclusions in sphalerite and associated gangue minerals (quartz, celestine, calcite and gypsum) shows that homogenisation temperatures ranged from 54 to 309 °C and cluster around 110 to 150 °C, with salinities of 1.6 to 18.0 wt.% NaCl equiv. Inert gas isotope studies from inclusions in ore- and gangue-minerals reveal 2.0 to 15.6% mantle He, 53% mantle Ne and a considerable amount of mantle Xe in the ore-forming fluids. The Pb-isotope composition of ores shows that the metal is mainly of mantle origin, mixed with a lesser amount of crustal lead. The widely variable and negative $\delta^{34}S$ values of Jinding sulphides suggest that thermo-chemical or bacterial sulphate reduction produced reduced sulphur for deposition of the Zn–Pb sulphides. The mixing of a mantle-sourced fluid enriched in metals and CO_2 with reduced sulphide-bearing saline formation water in a structural–lithologic trap may have been the key mechanism for the formation of the Jinding deposit.

The Jinding deposit differs from known major types of sediment-hosted Zn–Pb deposits in the world, including sandstone-type (SST), Mississippi Valley type (MVT) and sedimentary-exhalative (SEDEX). Although the fine-grained ore texture and high Zn/Pb ratios are similar to those in SEDEX deposits, the Jinding deposit lacks any exhalative sedimentary rocks. Like MVT deposits, Jinding is characterised by simple mineralogy, epigenetic features and involvement of basinal brines in mineralisation, but its host rocks are mainly sandstones and breccia-bearing sandstones. The Jinding deposit is also different from SST deposits with its high Zn/Pb ratios, among other characteristics. Most importantly, the Jinding deposit was formed in an intracontinental terrestrial basin

* Corresponding author.
E-mail address: chunji.xue@cugb.edu.cn (C. Xue).

0169-1368/$ - see front matter
doi:10.1016/j.oregeorev.2005.04.007

with an active tectonic history in relation to plate collision, and mantle-sourced fluids and metals played a major role in ore formation, which is not the case for SEDEX, MVT, and SST. We propose that Jinding represents a new type of sediment-hosted Zn–Pb deposit, named the 'Jinding type'.

Keywords: Jinding; Zn–Pb deposits; Fluid inclusions; Isotopes; Giant deposits; Lanping; Yunnan; China

1. Introduction

The Jinding Zn–Pb deposit is located in Lanping County, Yunnan Province, SW China, and it was discovered in 1960. Covering a surface area of about 8 km^2, the deposit has a reserve of ~200 Mt ore grading 6.08% Zn and 1.29% Pb, i.e., a metal reserve of ~15 Mt. Associated with Pb and Zn, there are a number of accessory metals, including Tl (8167 t grading 6 to 20 ppm), Cd (170,000 t at 0.01 to 0.2%), Ag (1722 t at 1 to 20 g/t, and as high as 156 g/t), and Sr (1.47 Mt at 13 to 18%). The Jinding deposit is the largest Zn–Pb deposit in China and probably the youngest giant sediment-hosted Zn–Pb deposit in the world (Xue et al., 2000; Khin Zaw et al., 2007-this volume).

The Jinding deposit occurs as tabular orebodies hosted within Early Cretaceous and Tertiary terrestrial clastic rocks in the Lanping–Simao Basin; no igneous rocks have been found nearby. The genesis of the deposit has been a subject of debate and controversy since the 1980s, and many models have been proposed to explain its origin. Two principal hypotheses, however, can be distinguished, namely a syngenetic (e.g., Shi et al., 1983; Zhao, 1989a; Qin and Zhu, 1991; Luo and Yang, 1994; Hu et al., 1998), and an epigenetic origin (Wu and Wu, 1989; Gao, 1989; Hu, 1989; Li and Kyle, 1997; Kyle and Li, 2002). Recent studies indicated that the mineral deposits in the Lanping–Simao Basin may have been linked with processes that occurred deep in the mantle; and lead isotopes and inert gas isotopes from ore minerals indicate involvement of mantle-derived fluids and metals in the formation of the Jinding deposit (Zhao, 1989b; Wang and Li, 1991; Zhou and Zhou, 1992; Zhang, 1993; Xue et al., 2000, 2002a, 2003, 2004).

This paper will review of the geological, fluid inclusion and isotopic characteristics of the Jinding Zn–Pb deposit, based on data compiled from the Chinese literature, including the authors' own work. The regional geology and the deposit geology of the Jinding deposit, including the occurrence of orebodies, alteration, and ore petrology are first described, prior to a detailed compilation and discussion of fluid inclusion and inert gas, Pb- and S-isotope data. The origin of the deposit is discussed in terms of the sources of the ore-forming fluids, sulphide and metals, the mechanism of ore precipitation, and the timing and structural control of mineralisation. Finally, we discuss the similarities and differences between Jinding and other sediment-hosted Zn–Pb deposits, and propose that the Jinding deposit represents a new type of sediment-hosted Zn–Pb deposit, named the 'Jinding-type', based on its distinctive combination of tectonic environments, structural control, host rocks, and significant involvement of mantle-derived fluids and metals.

2. Regional and ore district geology

2.1. Location and regional geological evolution

Geographically, the Jinding deposit is located in the Hengduanshan Mountains, a distinct NS-trending physiographic feature in South China. Tectonically, the Jinding deposit is located in the northern part of the Meso–Cenozoic Lanping–Simao Basin, which is an intracontinental basin developed on the Changdu–Lanping–Simao micro-plate between the Yangtze Plate to the east and the Tibet–Yunnan Plate to the west, separated by the Lancangjiang and Jinshajiang–Ailaoshan faults (Fig. 1) (Yin et al., 1990).

The Changdu–Lanping–Simao microplate was initially part of a landmass formed at about the end of the Silurian when the primary Tethys Ocean (Proterozoic–Early Palaeozoic) was closed. The landmass broke up along the Lancangjiang and Jinshajiang faults during the Late Palaeozoic when the Palaeo-Tethys Ocean was opened, forming a micro-plate with shallow marine basins and islands separated by oceans from the Yangtze Plate to the east and the Tibet–Yunnan Plate to the west. The Lancangjiang and Jinshajiang oceanic plates subducted eastward and westward beneath the micro-plate, respectively, forming volcanic islands along both edges of the microplate, which eventually became part of the Laurasian continent when the Palaeo-Tethys Ocean closed in the Late Permian or Early Triassic (Luo and Yang, 1994; Jin et al., 2003).

The development of the Lanping–Simao Basin on the Palaeo-Tethys basement was related to the

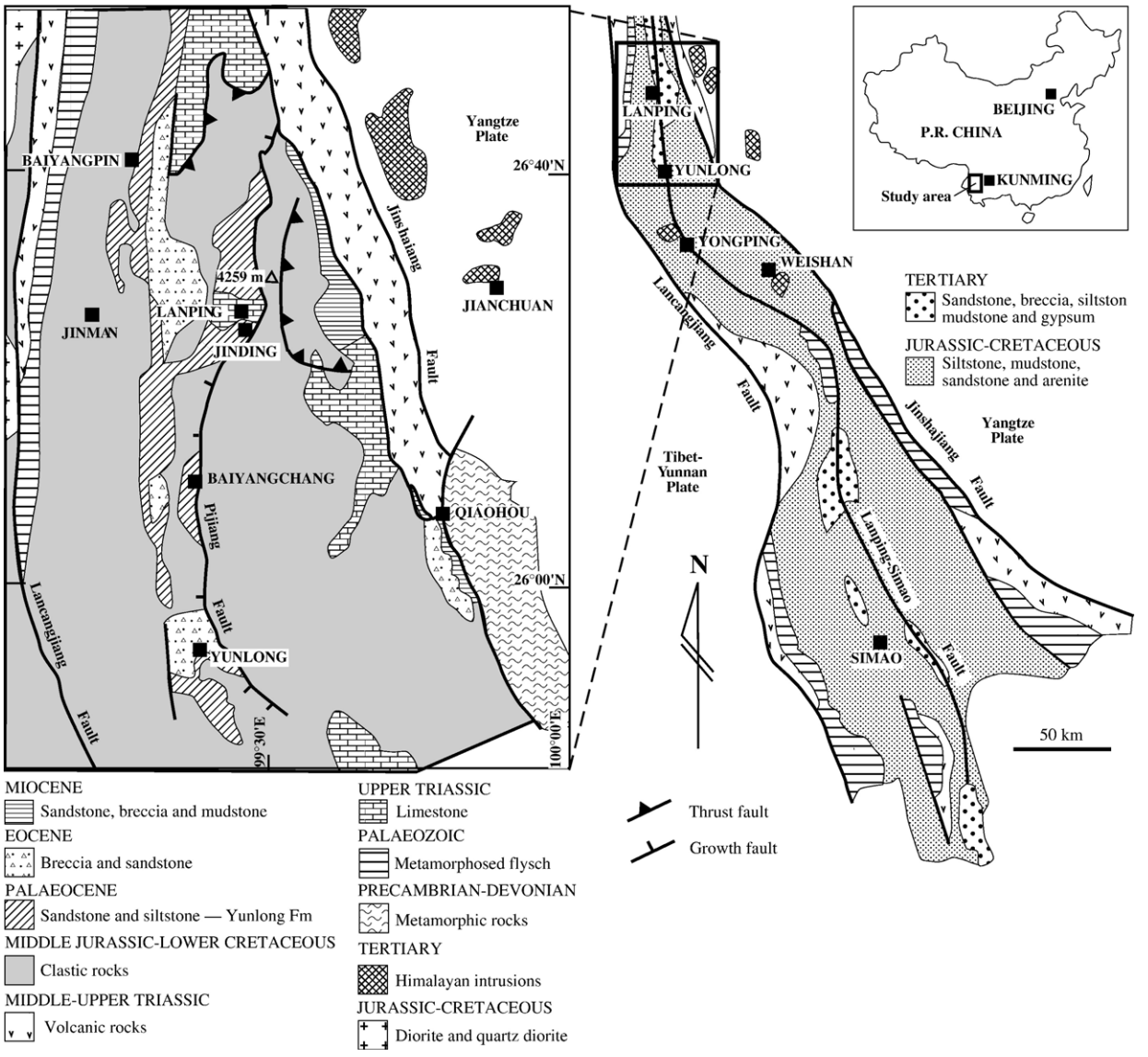

Fig. 1. Sketch geological map of the Lanping–Simao Basin in western Yunnan, China, showing the major structural features and the location of the Jinding deposit.

movement of the Indian and Eurasian Plates since the Mesozoic. The basin evolved from a remnant marine and marine-continental basin during the Triassic Period, through a continental depression basin during the Jurassic–Cretaceous Period, to a pull-apart continental basin during the Cenozoic Period (Xue et al., 2002b). Cenozoic tectonic events, which are particularly important to the formation of the Jinding Zn–Pb deposit, include regional westward thrusting that led to the formation of the Jinding nappe, a local continental crust uplifting that produced the Jinding dome (Xue et al., 2002b), and alkaline igneous activities between 68 and 23 Ma (see Xue et al., 2003) (Fig. 1).

2.2. Stratigraphy

The basement of the Lanping–Simao Basin consists of Proterozoic and Palaeozoic strata. The oldest strata are of Middle Proterozoic age and are distributed along the margins of the Lanping–Simao Basin. They are composed of sericite schist, marble, gneiss, amphibolite, biotite–plagioclase amphibolite, and the precursor lithologies are marine clastic rocks, carbonate and mafic volcanic rocks. This metamorphic basement is similar to the sequence that underlies the Yangtze Plate. The Palaeozoic strata are exposed in upwelling areas and the margin of the basin (Fig. 1). They are composed

of thick weakly metamorphosed marine flysch sequences that mainly consist of clastic rocks with some carbonate.

The Lanping–Simao Basin (Fig. 1) is essentially an intracontinental terrestrial basin. Six horizons of evaporites, dominantly of gypsum and halite, and occasionally also sylvite, have been found in the sequence. The total thickness of the evaporite layers may well exceed 2000 m in some places. The basin is filled with siliciclastic rocks, except for the lowest part of the sequence, and the Upper Triassic Sanhedong Formation (T_3s), which consists mainly of marine limestone and contains *Halobia ganziensis* Chen and some other fossils. There are several sedimentary gaps in the stratigraphic column of the basin (Qin and Zhu, 1991; Xue et al., 2002b). The Mesozoic–Cenozoic strata that outcrop in the ore district are summarized as follows (Xue et al., 2002b):

E_2g: Eocene Guolang Formation; argillaceous sandstone, siltstone, and gypsum.

E_1y: Palaeocene Yunlong Formation; breccias, sandstone and gypsum in the upper part, and siltstone, mudstone and gypsum in the lower part, containing *Djungarica* sp.

K_2h: Middle Cretaceous Hutousi Formation; quartz arenite and arkosic arenite.

K_1j: Lower Cretaceous Jingxing Formation; coarse-grained sandstone and arenite, containing coal seams and some plant fossils.

J_2h: Middle Jurassic Huakaizuo Formation; siltstone and mudstone with abundant fossils such as *Protocardia stricklandia* Morris and Lycett and *Darwinula lufengensis* Wang.

T_3m: Upper Triassic Maichuqing Formation; continental grey to black shale, siltstone and fine-grained sandstone, occasionally containing coal seams and *Equisettes* sp. and some other plant fossils.

T_3wl: Upper Triassic Waluba Formation; continental mudstone and siltstone.

T_3s: Upper Triassic Sanhedong Formation; marine limestone and dolomitic limestone; bitumen is commonly present in the limestone in the ore district.

2.3. Structures

There are three major regional faults trending north–northwest in the Lanping–Simao Basin, i.e., the Jinshajiang–Ailaoshan and Lancangjiang faults along the eastern and western margins of the basin, and the Lanping–Simao fault in the centre of the basin (Fig. 1). Geophysical and remote sensing data suggest that the faults cut deeply into the lower crust and upper mantle (Yin et al., 1990; Xue et al., 2002b; Jin et al., 2003), and show some hidden EW-trending structures (Xue et al., 2002b). The basin evolved into the Triassic remnant ocean basin, the Jurassic–Cretaceous continental depression basin and the Cenozoic pull-apart continental basin (Xue et al., 2002b). Mesozoic sedimentation in the basin was mainly controlled by the Lancangjiang, Jinshajiang–Ailaoshan faults, and the Cenozoic sediments were mainly distributed along the Lanping–Simao fault (Fig. 1) in the axial part of the basin (Yin et al., 1990; Xue et al., 2002b).

The most prominent structural features in the Jinding ore district are nappe structures produced by regional westward over-thrusting and a dome caused by uplifting (Figs. 2 and 3). The autochthon beneath the nappes displays a normal stratigraphic sequence consisting of Tertiary rocks (dominantly the Palaeocene Yunlong Formation, E_1y) and the underlying Middle Cretaceous Hutousi Formation (K_2h), with an unconformity between the two units, whereas the allochthon exhibits a reverse sequence consisting of Upper Triassic rocks (the Sanhedong Formation, T_3s) in the upper part and Lower Cretaceous rocks (the Jingxing Formation, K_1j) in the lower part. The reverse fault separating the allochthonous and autochthonous successions is called F_2 fault. A series of thrusts parallel to F_2 are developed within the nappes (Fig. 3). Thrusting may have been initiated during, and continued after, sedimentation of the Yunlong Formation (E_1y) (Xue et al., 2003).

The Jinding dome is roughly oval in shape, about 3 km long and 2.5 km wide with a NNE-trending axis. The dome was formed after the over-thrusting because both the allochthon and autochthon and the thrust faults are domed (Wu and Wu, 1989) (Fig. 3). As a result of the doming, the strata and the major thrust (F_2) now dips west in the western part of the Jinding ore district, north in the northern part and east in the eastern part, respectively. Therefore the autochthon, located in the central part of the ore district, comprises the core of the dome, and it is surrounded by the allochthon (Fig. 2).

2.4. Igneous rocks

Magmatic rocks of Upper Palaeozoic through Cenozoic are exposed along the margin of the Lanping–Simao Basin (Fig. 1), and Cenozoic igneous rocks also occur inside the basin, including the Zaojiaochang and Xiquechang intrusives in Yunlong County, the Zhuopan and Huanglianpu intrusives in Yongping

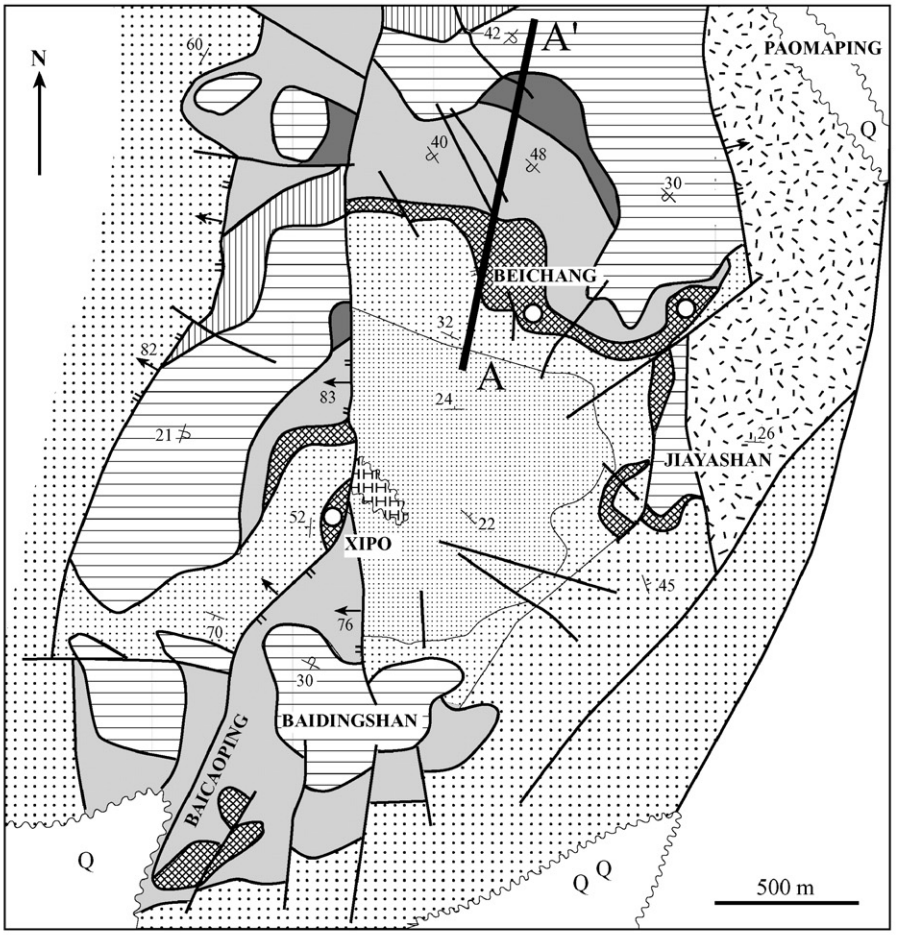

QUATERNARY
Q Pebble, sand and clay
EOCENE
Sandstone and siltstone — Guolang Fm
PALEOCENE
Undifferentiated — Yunlong Fm
Sandstone — Upper Yunlong Fm
Siltstone and mudstone — Lower Yunlong Fm
MIDDLE CRETACEOUS
Sandstone — Hutousi Fm
LOWER CRETACEOUS
Sandstone — Jingxing Fm
MIDDLE JURASSIC
Siltstone and mudstone — Huakaizuo Fm
UPPER TRIASSIC
Shale and siltstone — Maichuqing Fm

UPPER TRIASSIC
Mudstone and siltstone — Waluba Fm
Limestone — Sanhedong Fm

Zn-Pb orebody
Sample location
Reversed stratigraphic sequence
Normal stratigraphic sequence
Unconformity
Fault
Normal fault
Thrust fault

Fig. 2. Geological map of the Jinding Zn–Pb deposit, western Yunnan (after Geological Exploration Report of the Jinding Zn–Pb deposit, Third Team Geological Exploration, 1984).

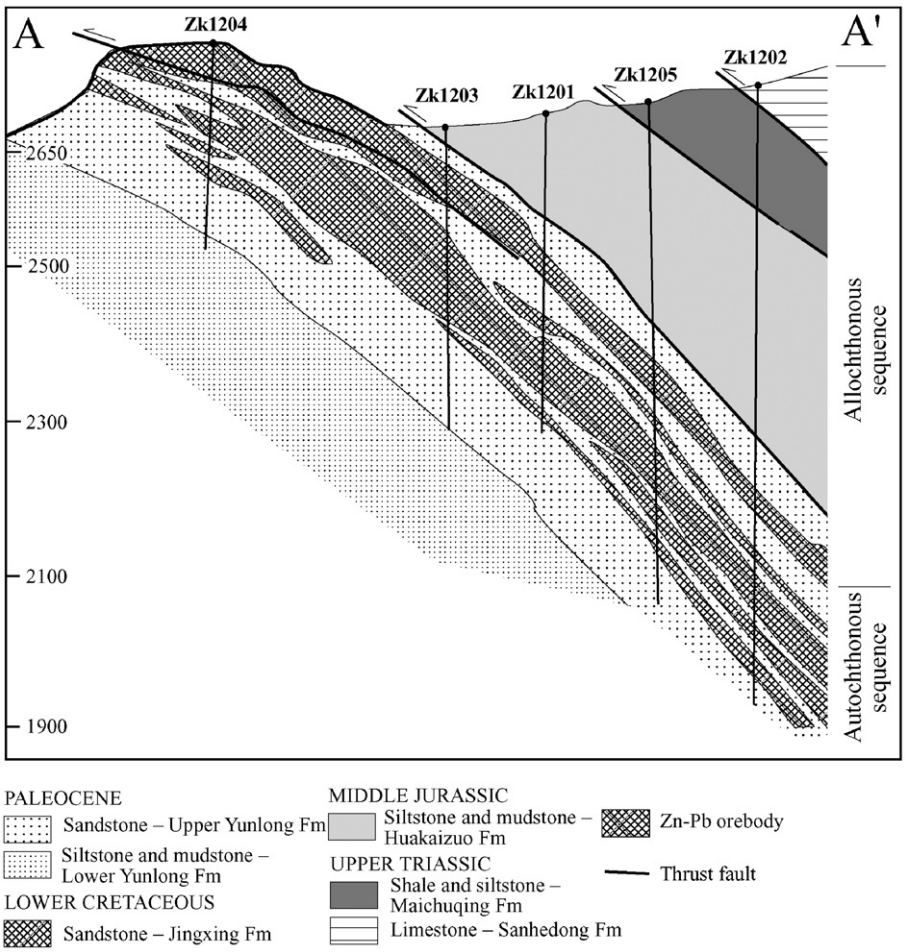

Fig. 3. Geological section of exploration line 12 through the Jinding Zn–Pb deposit, western Yunnan (after Geological Exploration Report of Jinding Zn–Pb Deposit, Third Geological Team, 1984).

County, and the Weishan intrusive in Weishan County. No igneous rocks have been found on the surface and underground in the Jinding ore district, but gravity surveys and remote sensing data suggest there is an intrusive body under the Jinding ore district (Zhang et al., 2000).

The Cenozoic igneous rocks distributed along Lanping–Simao fault include quartz syenite, beschtauite, granite porphyry, assyntite, essexite, alkaline basalt and trachyte. The isotope ages of these Cenozoic magmatic rocks range from 68 Ma to 23 Ma (Rb–Sr and U–Pb methods; Xue et al., 2003). Geochemical characteristics, e.g., $(^{87}Sr/^{86}Sr)_{initial}$ values of 0.7046 to 0.7084 and the presence of mantle-derived enclaves indicate that these Cenozoic magmatic rocks are of mantle origin (Lu and Qian, 1999).

Seismic studies in the Lanping–Simao Basin indicate that there are some lens-shaped, high temperature bodies in the crust with low velocity, which may be magma chambers formed from rising asthenosphere up to 15 to 20 km (Bian, 2000). A thermal metamorphic overprint is developed along the Lanping–Simao fault, such as at the Wuliangshan area, as a result of deep faulting, and hydrothermal fluids upwelled along the fault (Luo and Yang, 1994). This hydrothermal event occurred between 31 and 24 Ma (K–Ar dating of sericite; Xue et al., 2003).

3. Geology of the Jinding Zn–Pb deposit

3.1. Orebodies and wall-rock alteration

More than 100 orebodies have been discovered in the Jinding ore district, which is divided into six ore blocks distributed around the core of the Jinding dome. These ore blocks are Beichang, Paomaping, Jiayashan, Xipo,

Fengzishan and Baicaoping (Fig. 2). In fact, the ore blocks are segments of original orebodies cut by a series of radial faults. Among the ore blocks, Beichang is by far the most important one, accounting for 75% of the total reserve of the Jinding deposit (Third Geological Team, 1984; Luo and Yang, 1994).

The orebodies are mainly controlled by the F_2 thrust fault, and occur in both hanging- and footwall. The orebodies hosted in the Lower Cretaceous Jingxing Formation (K_1j) in the hangingwall are defined as the Upper Ore Zone and those hosted in the upper part of the Palaeocene Yunlong Formation (E_1y) in the footwall of F_2 are assigned to the Lower Ore Zone (Third Geological Team, 1984; Luo and Yang, 1994).

The orebodies in the Upper Ore Zone are usually tabular or stratabound in shape, since they are restricted to a sandstone layer (K_1j) where disseminated sulphide minerals occur in the sandstone. This style of mineralisation is referred to as sandstone-type (Third Geological Team, 1984; Qin and Zhu, 1991; Luo and Yang, 1994). The boundaries of an orebody and its host rock are gradual and determined by assay values. The No. 1 orebody in Beichang (Fig. 3) is the largest one in the Upper Ore Zone, accounting for 60% of the total reserve of the Jinding deposit (Luo and Yang, 1994). The cap rock of the No. 1 orebody consists of terrestrial sequences of the Middle Jurassic Huakaizuo Formation (J_2h), which is rich in argillaceous material and has a low permeability. A thin, 0.5 to 1 m, alteration halo is developed in the hangingwall contact with the orebodies, where the red beds are bleached and silicified (Third Geological Team, 1984; Luo and Yang, 1994).

The orebodies in the Lower Ore Zone are more variable in shape and occur as lenses, veins and various irregular bodies. Sulphide filling joints and fissures are also common. The ore in the Lower Ore Zone is referred to as breccia-type ore by local geologists because it occurs in breccias of the Yunlong Formation (Third Geological Team, 1984; Qin and Zhu, 1991; Luo and Yang, 1994).

3.2. Host rock and ore petrography

The sandstones of the Jingxing Formation (K_1j) which host the Upper Ore Zone mainly consist of quartz and siliceous lithic fragments, and a lesser amount of feldspar (Fig. 4A). The cements are generally carbonate (mainly calcite), together with some argillaceous material. In the low-grade ore the cements have been partially replaced by sulphides (pyrite, sphalerite, galena and marcasite), as well as celestine and minor barite (Fig. 4B). The cements have been almost entirely replaced, mainly by sulphides, in the high grade ore (Fig. 4C).

The host rocks of the Lower Ore Zone are breccia-bearing sandstones and breccias of the upper part of the Yunlong Formation (E_1y). The breccia fragments are poorly rounded and sorted, and mainly consist of bitumen-bearing limestones, which are similar to the limestone of the Upper Triassic Sanhedong Formation (T_3s). Other lithologies of the breccia-bearing host rocks include mudstone and siltstone (Fig. 4D). The interstitial materials of the breccias are fine-grained sandstone matrix. Ore minerals (sphalerite, galena, and pyrite) are disseminated in the interstitial sandstone matrix, and the mineralisation features are the same as those in the Upper Ore Zone. The breccia fragments are generally not mineralised (Third Geological Team, 1984; Xue et al., 2003).

3.3. Mineralogy

More than 30 primary minerals have been identified in the Jinding deposit, including sulphides, oxides, carbonates, sulphates, bitumen as well as native metals. The most common minerals in the primary ores are sulphides (sphalerite and galena). Pyrite (sometimes marcasite) is often present but in lesser amounts. Minor chalcopyrite, wurtzite, argentite and argentian tetrahedrite are also identified. Sulphide minerals are mostly fine-grained (50 to 100 μm) and some pyrites have colloform textures, but coarse-grained galena (up to 1 mm) is locally precipitated with calcite; coarse-grained pyrite occurs with celestine, and calcite and gypsum are also observed in late-stage veins or nodules. The contents of Ag, Tl and Cd in sulphides are very high (Third Geological Team, 1984). These metals mainly occur in galena (Ag: 47 to 135 g/t), pyrite and marcasite (Tl: 10 to 3850 ppm), and sphalerite (Cd: 0.10 to 1.64%). Silver is also identified in galena as fine inclusions of native silver and aphtonite. Cadmium mainly occurs as solid solution within sphalerite; traces of greenockite have been also found. No separate Tl-mineral phase has been identified so far (Xue et al., 2002c).

The sulphide ore is associated with quartz, celestine, calcite, bitumen, gypsum, anhydrite, hematite, and barite (Xue et al., 2002c). Quartz is mostly detrital in origin, and commonly shows signs of dissolution and secondary growth during mineralizing event. Some quartz was introduced during early silicification. Sulphate minerals, especially gypsum

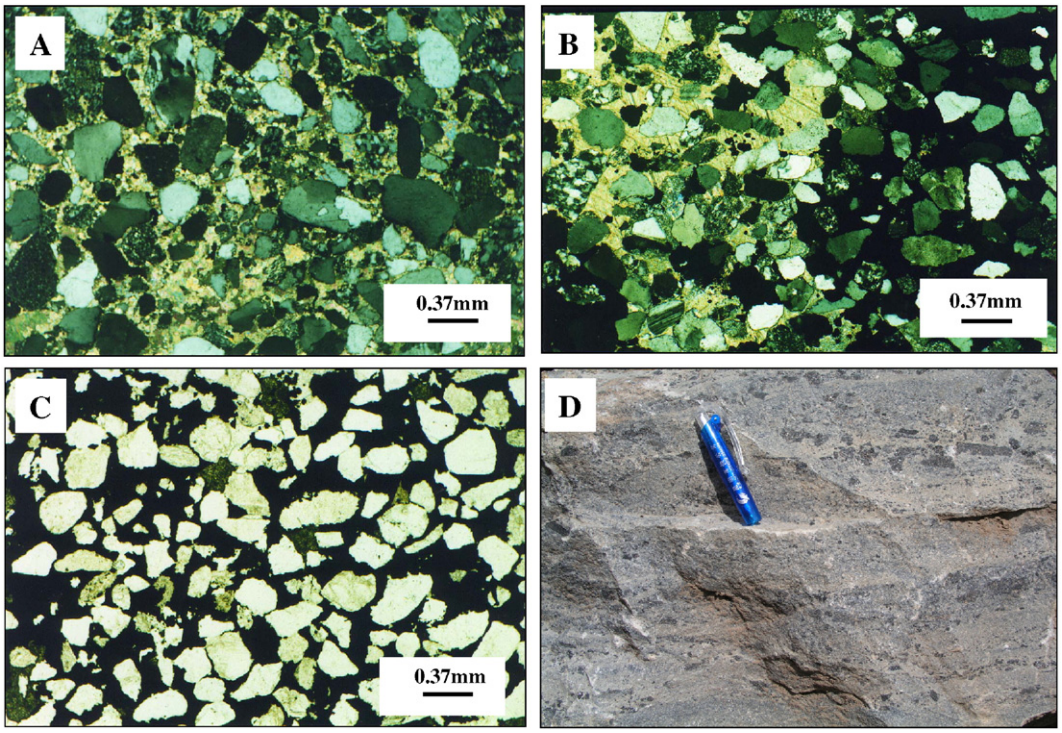

Fig. 4. Photomicrographs of host rock and ores from the Jinding Zn–Pb deposit, Yunnan, China. (A) Photomicrograph showing the sandstone host rock. Note the grains are mainly quartz and siliceous rock fragments, and a lesser amount of feldspar is also present. The cements are usually carbonates (mainly calcite). Transmitted, cross-polarised light. (B) Photomicrograph showing low-grade ore. Note the cements are partially replaced by sulphides (pyrite, sphalerite and galena) as well as celestine (and minor barite). Transmitted, cross-polarised light. (C) Photomicrograph showing high-grade ore. Note the cements are almost entirely replaced by sulphides. Transmitted, polarised light. (D) Photograph of ore-bearing breccia. Note the breccia fragments are not rounded and not sorted, and the main lithology is limestone and minor mudstone and siltstone. The interstitial material is fine-grained sandstone. The ore minerals (pyrite, sphalerite, galena) are disseminated in the interstitial sandstones, and the fragments are not mineralised.

and celestine, have at least two origins: those precipitated hydrothermally during ore formation, and those formed during sedimentation as part of the evaporite-bearing sequence of the Yunlong Formation (E_1y). Bitumen (asphalts and heavy oils) occurs in the veins and dissemination in ores, in both the Upper and the Lower Ore zones. Disseminated bitumen occurs in the sandstone matrix and breccia-type ores, which commonly have an oily smell. Bitumen in veins in the ore and host rocks is interpreted to have formed from remobilization of previous bitumen, and is commonly associated with celestine, calcite and gypsum (Xue et al., 2002c).

The Jinding hydrothermal mineralisation is divided into three stages based on paragenetic studies and intergrowth relationships of the primary minerals: (I). 'quartz+sphalerite+galena' stage; (II) 'sphalerite+galena+celestine' stage, and (III) 'galena+calcite+celestine+gypsum' stage. The galena of the third stage is coarse-grained and associated with calcite in veins and vugs, whereas the galena of the earlier stages is fine-grained and disseminated. The celestine of the third stage occurs in veins and is associated with the remobilised bitumen, which is different from the sedimentary celestine in strata and the disseminated hydrothermal celestine in the ore. Pyrite occurs in all stages, but is most common in the second and the third stages. The disseminated bitumen formed before the Zn–Pb mineralisation was hydrothermally matured during the mineralisation, and the hydrothermally remobilised bitumen developed in the third stage.

3.4. Zoning

There is a distinct zoning of mineral assemblages, both vertically and laterally (Fig. 5), in the Jinding ore district. A general sequence of mineral assemblages from the east to the west and upward is as follows: celestine–gypsum–barite → pyrite–marcasite →

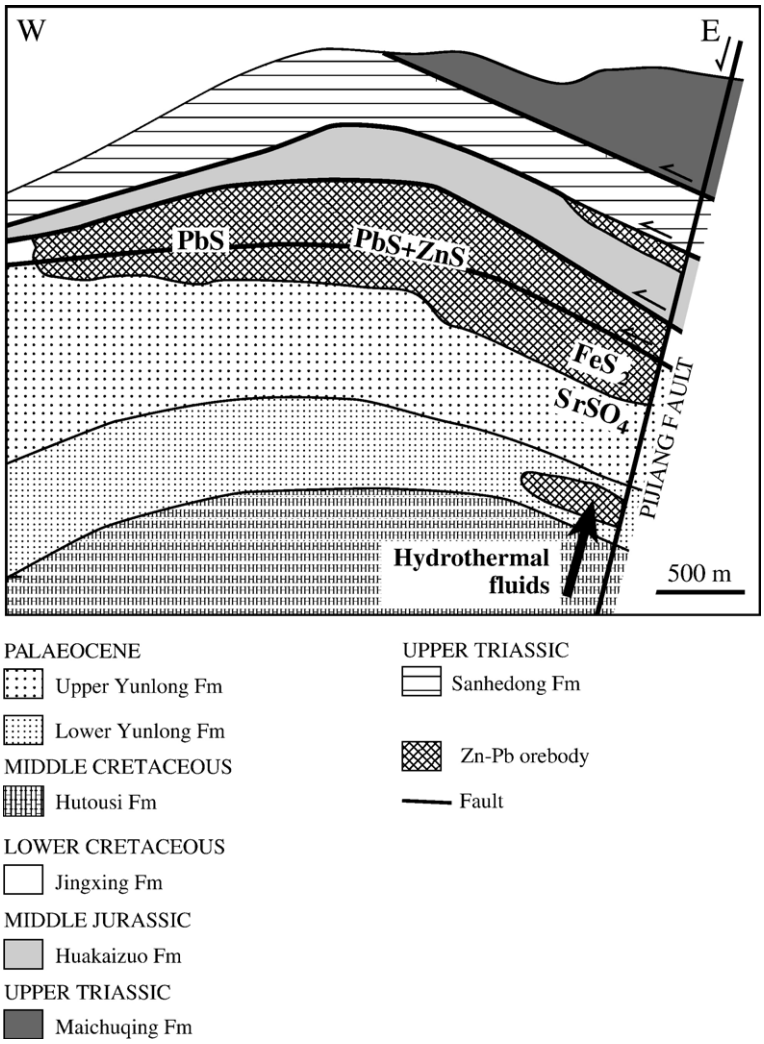

Fig. 5. A sketch cross-section showing mineral zoning in the Jinding Zn–Pb deposit, Yunnan, China.

sphalerite→sphalerite–galena→galena (Third Geological Team, 1984; Luo and Yang, 1994; Xue et al., 2002c). Corresponding to this trend, there is a change in element association Sr–Ca–Ba→Fe–Tl→Zn–Cd→Zn–Pb–Cd–Ag→Pb–Ag. The Zn/Pb ratios change from 7.8 at Jiayashan (east), through 4.9 at Beichang (central north), to 0.3 at Fengzishan (west) (Luo and Yang, 1994; Xue et al., 2002c; Kyle and Li, 2002).

3.5. Oxidised zone and supergene enrichment

Due to high relief, mild temperature all year around, and a large amount of annual precipitation, the oxidised zone is well-developed in the Jinding deposit, and extends to a depth of more than 100 m. The oxidised ore zone accounts for 40% or more of the total ore reserve, and therefore is economically very important. The ore in this zone consists of supergene carbonates such as smithsonite, hydrozincite, cerussite and strontianite, as well as many other supergene minerals such as calamine, plumbojarosite, limonite, celestine, barite, and calcite. Generally the ore in this zone has a higher grade than the primary ore. Supergene sulphide enrichment is also occasionally observed, but is of less significance (Third Geological Team, 1984).

4. Fluid inclusion studies

4.1. Fluid inclusion petrography and microthermometry

Fluid inclusions have been found in sphalerite and associated quartz, celestine, calcite and gypsum in the

Jinding ores. The fluid inclusions are ellipsoidal and amygdaloidal in shape, and show a size variation from 3 to 20 μm (Fig. 6). Fluid inclusions distributed in healed fractures are not studied. Fluid inclusions occurring in clusters, in isolation and along growth zones are considered primary and have been studied.

Three types of fluid inclusions have been identified at room temperature and they are single-, two- and three-phase inclusions (Fig. 6). The single-phase inclusions are from 3 to 10 μm and are found in calcite, gypsum and celestine. The two-phase inclusions range in size from 5 to 16 μm, and consist of LH_2O and VH_2O, with the volume of LH_2O being >65 vol.%. They are found

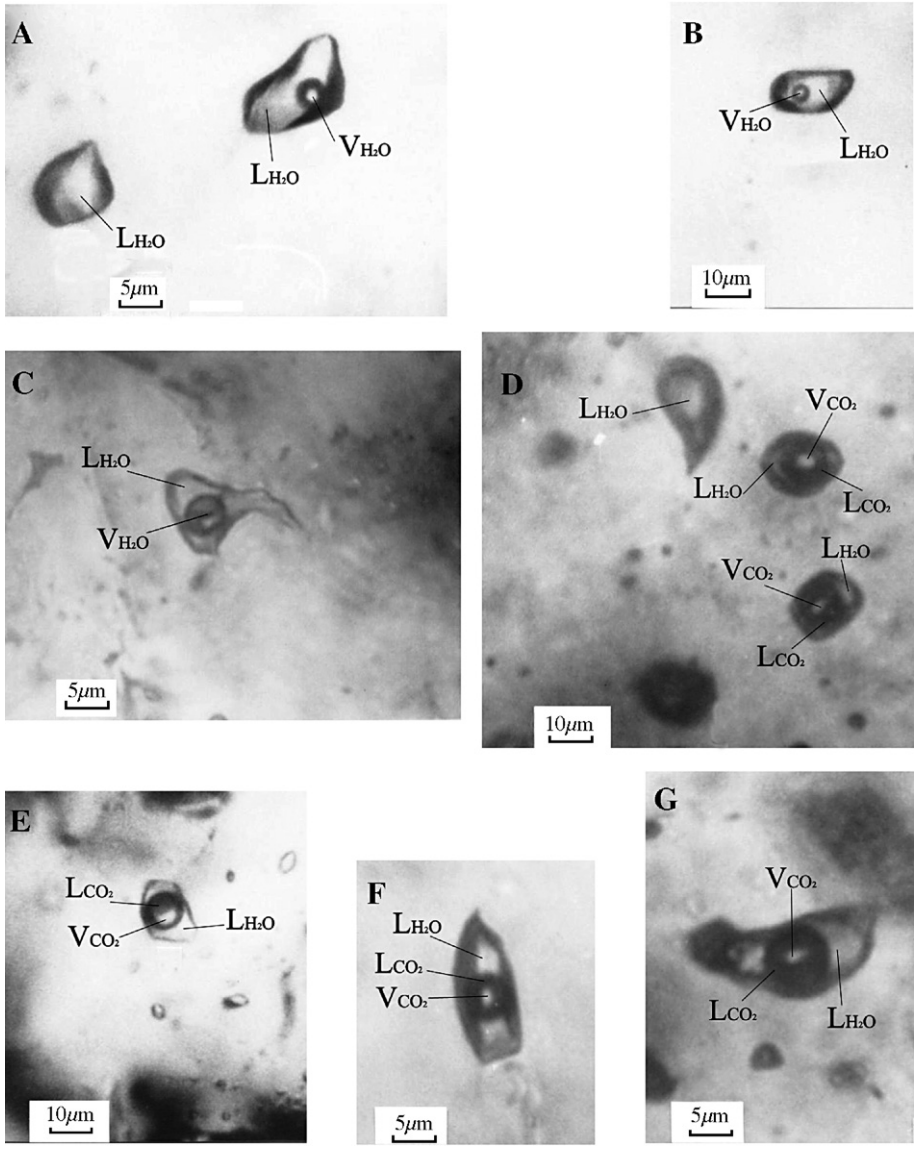

Fig. 6. Photomicrographs of the fluid inclusion types from sphalerite and associated quartz, celestine and calcite in the Jinding ores (room temperature). (A) Single-phase liquid H_2O inclusion (left) and a two-phase vapour–liquid H_2O inclusion (right) in celestine. (B). Two-phase vapour–liquid H_2O inclusion in calcite. (C) Two-phase vapour–liquid H_2O inclusion in quartz. (D) Single-phase liquid H_2O inclusion (upper) in quartz and two three-phase liquid H_2O–liquid CO_2–vapour CO_2 inclusions (the other two on right) in sphalerite. (E) Three-phase liquid H_2O–liquid CO_2–vapour CO_2 inclusion in quartz. (F) Three-phase liquid H_2O–liquid CO_2–vapour CO_2 inclusion in celestine. (G) Three-phase liquid H_2O–liquid CO_2–vapour CO_2 inclusion in celestine.

in quartz, sphalerite, celestine and calcite. The three-phase inclusions are composed of LH_2O, LCO_2 and VCO_2, with the volume of CO_2 being about 40 to 80 vol.% (Xue et al., 2002a) and range in size from 6 to 20 μm. They are found in quartz, sphalerite and celestine (Fig. 6).

Microthermometric studies were carried out at the fluid inclusion laboratory, Chang'an University, using

Table 1
Microthermometric data of fluid inclusions in the Jinding Zn–Pb deposit

Sample no.	Ore-block	Mineral	T_{ice} (°C)	T_h (°C)	Slt (wt% NaCl eq.)	Sample no.	Location	Mineral	T_{ice} (°C)	T_h (°C)	Slt (wt% NaCl eq.)
Pmp05-6	Paomaping	Quartz		189		Jysh51-h	Jiayashan	Sphalerite	−8.0	126	9.3
		Quartz	−8.5	181	9.8			Sphalerite	−13.0	158	13.6
		Celestine	−7.9	181	9.1			Celestite	−3.5	161	4.3
Pmp20-1	Paomaping	Sphalerite	−8.2	234	9.5			Celestite	−2.5	180	3.2
		Sphalerite	−8.6	204	9.9			Celestite	−6.2	174	7.1
		Celestite	−9.3	170	10.7			Quartz	−9.1	166	10.5
		Celestite	−3.9	133	4.8	Jysh01-9	Jiayashan	Calcite	−3.8	140	4.7
Jysh004	Jiayashan	Quartz		250				Calcite	−3.8	162	4.7
		Quartz	−4.7	176	5.6			Calcite	−3.1	256	3.9
		Quattz		175		Jysh21	Jiayashan	Gypsum	−3.2	141	4.0
		Quartz	−4.9	176	5.9			Gypsum	−3.1	138	3.9
		Quartz		165		Bch25-4	Beichang	Quartz	−10.2	157	11.7
Jysh48-1	Jiayashan	Celestite	−7.9	309	9.1			Sphalerite		190	
		Celestite	−3.7	275	4.6			Sphalerite	−8.5	185	9.8
		Celestite	−4.9	262	5.9			Sphalerite		175	
Jysh8-09	Jiayashan	Sphalerite	−12.0	174	13.6			Celestite	−5.1	180	6.1
		Sphalerite	−4.8	195	5.8	Bch60-3	Beichang	Calcite	−4.1	240	5.0
		Sphalerite	−4.0	196	4.9			Calcite	−3.2	135	4.0
		Sphalerite	−6.7	190	7.8			Calcite	−1.2	135	1.8
		Celestite	−6.2	280	8.4	Bch206	Beichang	Celestite	−1.0	120	1.6
Jysh37-5	Jiayashan	Sphalerite	−4.2	182	5.1			Celestite	−2.8	119	3.6
		Sphalerite	−12.4	194	14.1			Celestite	−1.3	146	1.9
		Sphalerite		185				Celestite		120	
		Celestite	−3.5	262	4.3			Celestite		115	
Bch006	Beichang	Sphalerite	−3.3	143	4.1	Xp-009	Xipo	Calcite	−2.8	87	3.6
		Celestite	−4.0	161	4.9			Calcite	−2.4	87	3.1
Bch43	Beichang	Calcite	−2.5	131	3.2			Calcite	−2.8	101	3.6
		Calcite	−1.1	135	1.7			Calcite	−3.5	99	4.3
		Calcite	−2.8	130	3.6			Calcite		89	
Bch52-5	Beichang	Gypsum		132		Xp56-12	Xipo	Calcite		87	
		Gypsum	−1.0	130	1.6			Calcite	−2.3	77	3.0
		Gypsum	−1.8	116	2.5			Calcite	−4.6	75	5.5
		Gypsum	−2.1	112	2.8			Calcite		86	
Xp00-9	Xipo	Sphalerite	−3.3	133	4.1	Fzsh55	Fengzishan	Sphalerite	−16.0	115	18.0
		Celestine	−12.8	106	14.5			Celestite	−13.0	98	14.7
Xp01-2	Xipo	Calcite	−3.5	129	4.3	Fzsh102	Fengzishan	Calcite	−5.1	120	6.1
		Calcite	−3.9	110	4.8			Calcite	−3.6	83	4.4
		Calcite	−4.9	128	5.9			Calcite	−4.0	73	4.9
		Calcite	−4.7	114	5.6			Calcite		70	
		Calcite		105				Calcite		67	
		Calcite		91				Calcite	−1.1	59	1.7
Xp99-23	Xipo	Gypsum	−3.2	92	4.0			Calcite	−2.3	88	3.0
		Gypsum	−4.4	101	5.3			Calcite		85	
		Gypsum	−2.1	99	2.8			Calcite		79	
		Gypsum		98		Fzsh01-22	Fengzishan	Gypsum	−3.9	98	4.8
Xp-007	Xipo	Sphalerite	−14.5	128	16.4			Gypsum	−1.9	66	2.6
		Celestite		105				Gypsum	−4.6	54	5.5

Notes: T_{ice} (°C)—freezing temperature; T_h (°C)—homogenization temperature; Slt (wt% NaCl eq.)—salinity. Cooling–heating stage: LINKAM-TMS94 Type in Chang'an University.

a LINKAM-TMS94 cooling–heating stage. Precision is 0.1 °C for temperatures <30 °C, and 1 to 2 °C for temperatures >30 °C. Seventy-three freezing-temperature and 94 homogenisation temperature data have been obtained (Table 1).

4.2. Homogenisation temperatures

The homogenisation temperatures range from 54 to 309 °C (Table 1). The average homogenisation temperatures are 182 °C in quartz, 154 °C in sphalerite, 140 °C in celestine, 126 °C in calcite and 98 °C in gypsum. Three homogenisation temperature peaks are revealed in the stacked histogram (Fig. 7), i.e., a 170 to 190 °C peak, mainly consisting of inclusions in quartz, sphalerite and celestine, a 110 to 140 °C peak of inclusions in sphalerite, celestine and calcite, and an 80 to 100 °C peak of inclusions in calcite and gypsum. These peaks broadly correspond to the three hydrothermal stages recognized by ore petrography and mineral paragenesis. The minor 230 to 280 °C population (Fig. 7) is treated as an outlier and will not be discussed further in this paper.

There is a general westward decrease in homogenisation temperatures in the Jinding ore district. The average homogenisation temperature of all the T_h measurements changes from 170 °C in the eastern part of the ore district (Paomaping, Jiayashan and Beichang) to 95 °C in the western part (Xipo and Fengzishan). The average homogenisation temperatures in individual minerals also show similar trends: 182 °C (east)–125 °C (west) for sphalerite, 182 °C (east)–103 °C (west) for celestine, 163 °C (east)–88 °C (west) for calcite, and 111 °C (east)–74 °C (west) for gypsum.

4.3. Salinity

The first melting temperatures of the aqueous fluid inclusions range from −17 to −23 °C, suggesting a NaCl–(KCl)–H_2O system. The salinities range from 1.6 to 18.0 wt.% NaCl equiv. (Table 1), with an average of 6.1 wt.% NaCl equiv. and a mode around 4 to 5 wt.% NaCl equiv. (Fig. 8). The average salinity is 8.7 wt.% NaCl equiv. for fluid inclusions in quartz, 10.5 wt.% NaCl equiv. in sphalerite, 10.0 wt.% NaCl equiv. in celestine, 5.2 wt.% NaCl equiv. in calcite, and 3.6 wt.% NaCl equiv. in gypsum. The difference in salinity between different minerals can be recognized in Fig. 8.

Salinity values of all the measurements also show a systematic increase from east to west across the district. The average salinity is 5.8 wt.% NaCl equiv. in the east and 9.6 wt.% NaCl equiv. in the west. The average salinities in individual minerals are as follows (all in wt.% NaCl equiv.): 8.3 (east)–12.8 (west) for sphalerite; 5.4 (east)–14.6 (west) for celestine, 3.6 (east)–6.9 (west) for calcite, and 3.0 (east)–4.2 (west) for gypsum (calculated from Table 1).

The westward decrease in homogenisation temperature and corresponding increase in salinity indicates

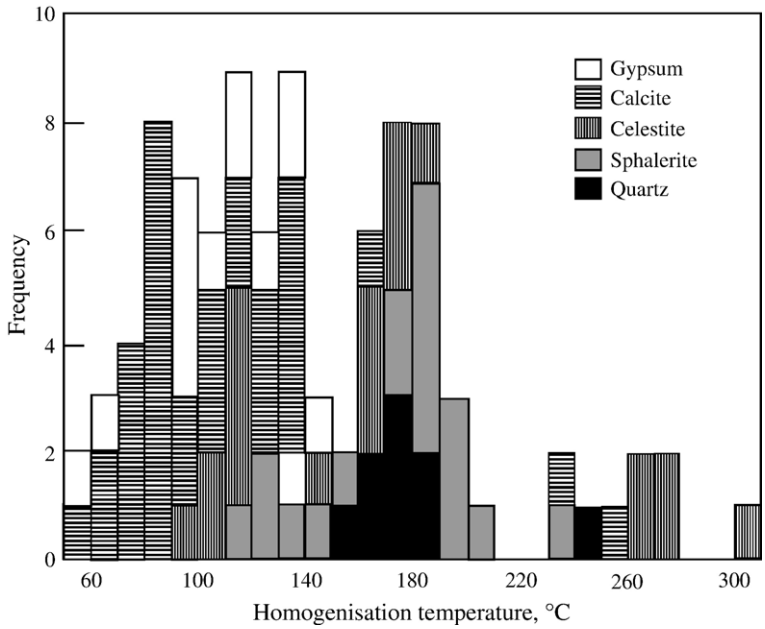

Fig. 7. Histogram of homogenisation temperatures of fluid inclusions in the Jinding ores, Yunnan, China.

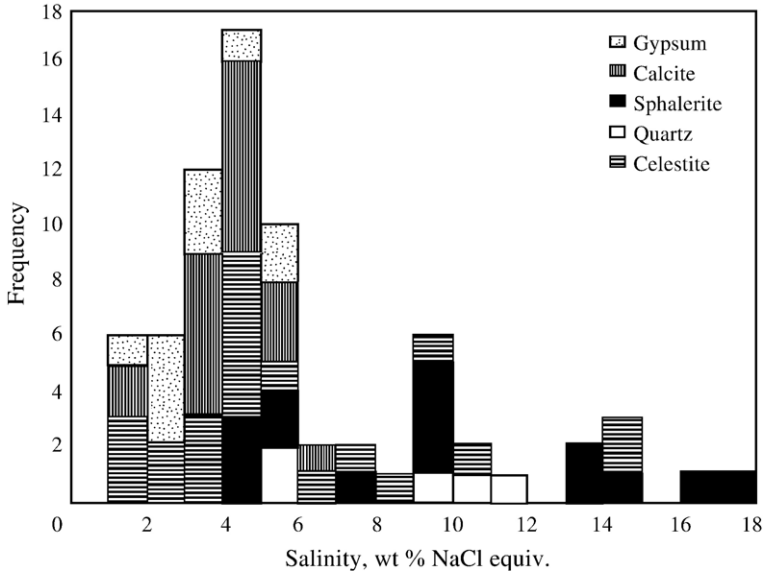

Fig. 8. Histogram of salinity of fluid inclusions in the Jinding ores, Yunnan, China.

negative correlation, which is also reflected in the T_h–salinity diagram, especially for data from sphalerite, celestine and quartz (Fig. 9). This negative T_h–salinity trend probably resulted from the mixing of a high-temperature low-salinity fluid with a low-temperature high-salinity fluid during the main stage of mineralisation. The low-temperature, low-salinity data clustered on the lower left corner of Fig. 9, mainly derived from calcite and gypsum, probably reflects the conditions in the late stage of the hydrothermal system.

5. Isotope studies

5.1. He-, Ne-, Xe-isotopes of fluid inclusions

Noble gas (He, Ne, and Xe) isotopes were studied for fluid inclusions hosted in pyrite, sphalerite, celestine and barite formed in the main ore-forming stage. Noble gas isotopic compositions were analysed at the Isotope Laboratory, Chinese Academy of Geological Sciences, Beijing. First, the samples were washed with acetone

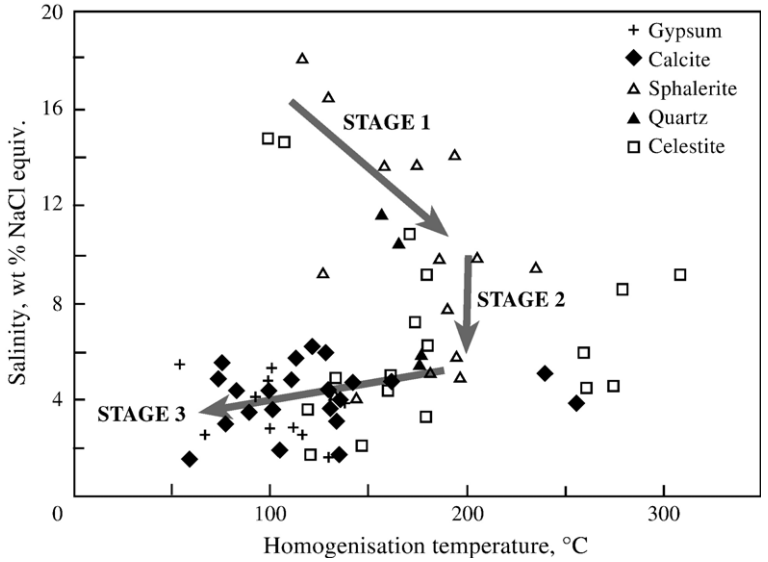

Fig. 9. Plot of homogenisation temperature (T_h) vs. salinity in the Jinding Zn–Pb deposit, Yunnan, China.

Table 2
Helium, neon, xenon isotopic compositions of fluid inclusions of main ore-forming stages in the Jinding Zn–Pb deposit, Yunnan, China

Sample no.	K_2J-3	BC-3	XP-2	JYS-3
Host mineral	Sphalerite	Pyrite	Barite	Celestine
^3He ($\times10^{-15}$ cm^3/g)	22.71	32.55	452.58	63.69
^4He ($\times10^{-8}$ cm^3/g)	8.41	7.03	39.70	9.58
^{20}Ne ($\times10^{-8}$ cm^3/g)	0.43	0.38	19.10	1.08
^{129}Xe ($\times10^{-13}$ cm^3/g)	43.94	25.09	52.70	na
^{134}Xe ($\times10^{-13}$ cm^3/g)	16.67	9.40	22.82	na
$^3He/^4He$ ($\times10^{-7}$)	2.70	4.63	11.40	6.67
Rc/Ra	0.19	0.33	0.82	0.48
$^{20}Ne/^{22}Ne$	10.72	10.62	10.82	10.57
$^{21}Ne/^{22}Ne$	0.03	0.03	0.03	0.03
$^{129}Xe/^{130}Xe$	6.61	6.86	5.80	na
$^{134}Xe/^{130}Xe$	2.55	2.57	2.53	na

The gases isotopic volumes in the table are obtained under standard atmosphere. The working standard is Beijing atmosphere. Rc is $^3He/^4He$ of the sample, Ra is $^3He/^4He$ of the air (1.40×10^{-6}). The samples were analysed by Song, H. B. and Li, Y. H. in Open Laboratory of Isotopic Geology, Chinese Academy of Geological Sciences. The analyzed method is progressive heating, and the precision is ±0.01. "na" not analysed.

and dried at 90 °C for 48 h in an oven in order to release atmospheric gases. The oven was connected to the apparatus which was used to gather, separate and purify the noble gases. Second, the gas gathering system was evacuated to 10^{-8} MPa, and the samples were heated to 450 °C under vacuum to extract the gases in fluid inclusions, and then the gases were separated and purified. Third, the pure He, Ne and Xe were analysed in a noble gas spectrometer (model MI-1201IG). Faraday cups and photoelectric multipliers were used to receive the isotopes. The multiplier's resolution power was 760 (up to 1300); precision was ±0.01.

Results of He, Ne, and Xe isotope compositions of the fluid inclusions are shown in Table 2 and Figs. 10, 11, and 12. The analysed isotopic compositions are believed to represent the original ore-forming fluids because the host sulphate and sulphide minerals provided a very good seal for noble gases (Trull et al., 1991; Baptiste and Fouquet, 1996). The contents of U, Th, Mg, F and Pu, which can produce radiogenetic daughter products, are very low in the host minerals, and the contents of U, Th, and Pu in the fluid inclusions are close to zero. Th is not readily dissolved in hydrothermal solution and thus has almost no influence on the initial isotopic ratios (Norman and Musgrave, 1994; Xue et al., 2000).

Without the influence of atmospheric ^3He, the helium in the ore-forming fluids in the Jinding deposit could have been derived either from the crust or from the mantle (Stuart and Turner, 1992; Stuart et al., 1995). Mantle helium is the remainder of the earth's primary helium, which is characterised by an enrichment of ^3He compared to crustal helium. The $^3He/^4He$ ratio of the mantle is 6–7 Ra (Ra is the $^3He/^4He$ ratio of the air, i.e.,

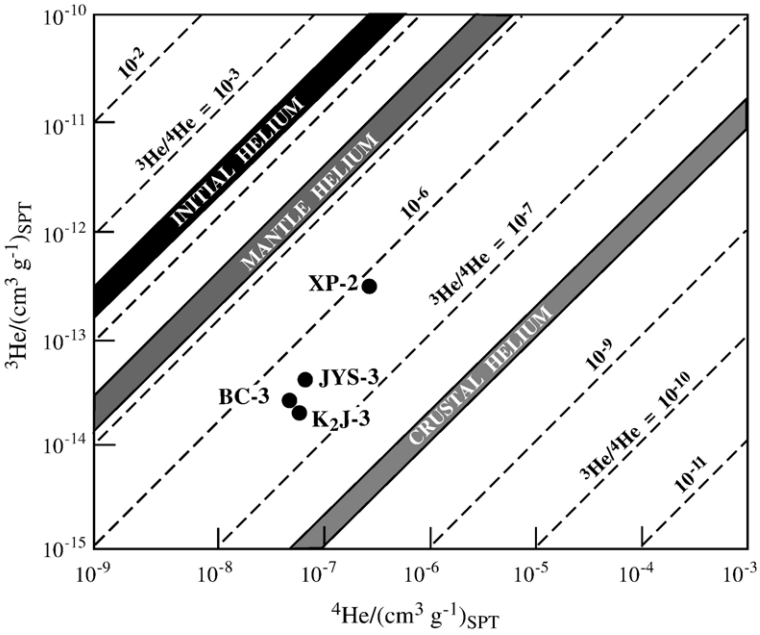

Fig. 10. Helium isotopic compositions of fluid inclusions and comparison with some natural systems and their evolutionary trends (after Mamyrin and Tolstikhin, 1984). Sample numbers same as in Table 2.

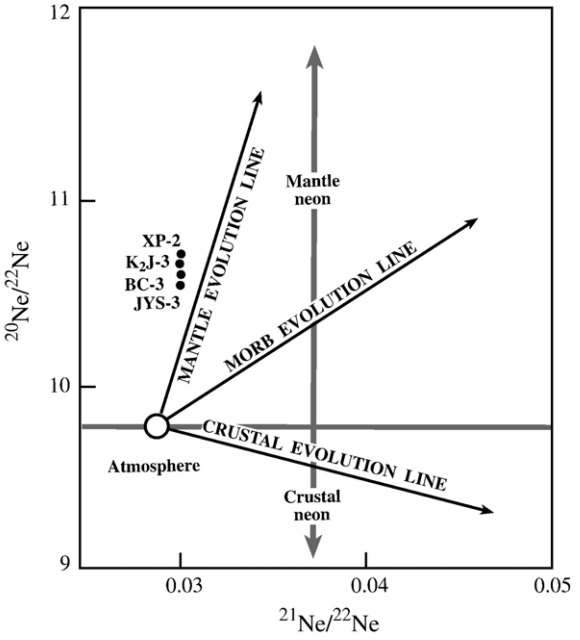

Fig. 11. Plot of $^{21}Ne/^{22}Ne$ vs. $^{20}Ne/^{22}Ne$ of fluid inclusions from Jinding and comparison with different source areas of the Earth (modified after Sarda et al., 1988; Kennedy et al., 1990; Ballentine and O'Nions, 1991; Lollar et al., 1994; Swindle et al., 1995; Ballentine et al., 1996; Fisher, 1997; Harrison et al., 1999; Hanyu et al., 1999).

1.40×10^{-6}; Stuart and Turner, 1992; Stuart et al., 1995). Crustal helium is the product of U and Th decay or of their neutron reactions (mainly with Li). The crustal $^{3}He/^{4}He$ ratio depends on the abundances of U, Th and Li, and is typically in the range of 0.01 Ra to 0.05 Ra (Stuart et al., 1995). Our data show that the ore fluids have $^{3}He/^{4}He$ ratios from 0.19 Ra to 0.82 Ra (Table 2), which are much higher than that of the crust. On the helium isotope evolution diagram of natural systems (Fig. 10; Mamyrin and Tolstikhin, 1984), the Jinding data fall in a region between the crust and the mantle, indicating mixing of mantle- and crust-derived gases. Assuming a $^{3}He/^{4}He$ ratio of 7 Ra and 0.01 Ra for the mantle and crust, respectively, we calculate that the amount of mantle helium in the ore-forming fluids is in the range of 2.0 to 15.6%.

The neon isotope ratios of the atmosphere are 9.8 for $^{20}Ne/^{22}Ne$ and 0.029 for $^{21}Ne/^{22}Ne$ (Kennedy et al., 1990). $^{20}Ne/^{22}Ne$ and $^{21}Ne/^{22}Ne$ of the solar wind are 13.5 to 14.0 and 0.0305 to 0.034 (the earth initial value, Harrison et al., 1999), respectively. The mantle neon is the remainder of earth primary Ne, thus the isotope ratios should be close to those of the solar wind. The $^{20}Ne/^{22}Ne$ ratios of mantle fluids are higher than 9.80, with an extreme of 13.2, and the $^{21}Ne/^{22}Ne$ values are clustered around 0.058 to 0.068 (Staudacher and Allègre, 1982; Sarda et al., 1988; Ballentine and O'Nions, 1991; Fisher, 1997; Hanyu et al., 1999; Harrison et al., 1999). In contrast, crustal Ne is the decay products of ^{17}O, ^{18}O, ^{24}Mg, ^{19}F, and ^{25}Mg (Kennedy et al., 1990). The determined and calculated values (based on crustal O/F ratios) are very close, with $^{20}Ne/^{22}Ne$ from 0 to 0.3 and $^{21}Ne/^{22}Ne$ from 0.1 to 0.47 (Kennedy et al., 1990; Ballentine and O'Nions, 1991; Lollar et al., 1994; Swindle et al., 1995; Ballentine et al., 1996). The neon isotopic compositions in the ore-forming fluids at Jinding deposit are 10.45 to 10.83 for $^{20}Ne/^{22}Ne$ and 0.027 to 0.03 for $^{21}Ne/^{22}Ne$, indicating the presence of some mantle neon in the ore-forming fluids.

The origin and character of neon in the mantle and the crust are distinct, and have different evolutionary trends, and thus have different isotopic compositions. A review of research into Ne geochemistry (Sarda et al., 1988; Kennedy et al., 1990; Ballentine and O'Nions, 1991; Lollar et al., 1994; Swindle et al., 1995; Ballentine et al., 1996; Fisher, 1997; Harrison et al., 1999; Hanyu et al., 1999) shows that the crust, the MORB, and the mantle have distinct Ne isotopic composition and evolution trends (Fig. 11). The Ne isotopic compositions in the ore-forming fluids in the Jinding deposit are close to the mantle Ne isotopic evolution line, and the variation of $^{21}Ne/^{22}Ne$ ratios is very small, unlike the crustal Ne isotopic composition features which show a negative correlation between $^{21}Ne/^{22}Ne$ and $^{20}Ne/^{22}Ne$ (Fig. 11). Using the Ne isotope model of Ballentine and O'Nions (1991), our calculations suggest that there is 53% mantle Ne in the ore-forming fluids of the Jinding deposit.

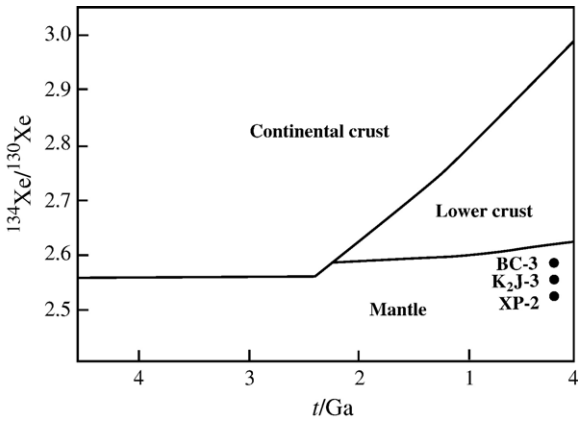

Fig. 12. $^{134}Xe/^{130}Xe$ ratios of fluid inclusions from Jinding in comparison with the evolution of different source areas in the Earth (after Staudacher and Allègre, 1982). It is assumed that $(^{238}U/^{130}Xe)_{continental\ crust}=3.5\times10^{7}$; $(^{238}U/^{130}Xe)_{lower\ crust}=0.5\times10^{7}$ and $(^{238}U/^{130}Xe)_{upper\ mantle}=3.8\times10^{5}$.

^{134}Xe is the decay product of ^{244}Pu and ^{238}U. ^{244}Pu is a short-lived isotope with a half-life of 82 Ma, so ^{134}Xe evolution (Fig. 12) of the fluids in different source areas of the earth should be controlled mainly by the decay of ^{238}U (Staudacher and Allègre, 1982). Three Xe isotopic compositions of fluid inclusions in sphalerite, pyrite and barite from Jinding (Table 2) fall in the mantle evolution region (Fig. 12), indicating considerable amounts of mantle Xe in the ore-forming fluids.

Table 3
Ore lead isotopic compositions of the Jinding Zn–Pb deposit, Yunnan, China

Sample no.	Mineral	^{206}Pb/^{204}Pb	^{207}Pb/^{204}Pb	^{208}Pb/^{204}Pb	Sample no.	Mineral	^{206}Pb/^{204}Pb	^{207}Pb/^{204}Pb	^{208}Pb/^{204}Pb
After Bai et al. (1985)					After Zhou and Zhou (1992)				
BTW1	Galena	18.444	15.625	38.584	Yn-9	Galena	18.390	15.600	38.540
BTW	Sphalerite	18.566	15.627	38.675	Yn-10	Galena	18.170	15.341	37.802
BTW2	Galena	18.394	15.583	38.470	Yn-13	Galena	18.311	15.470	38.141
BTW2	Sphalerite	18.543	15.676	39.046	Yn-26	Galena	18.360	15.580	38.440
BTW3	Pyrite	18.413	15.597	38.483	Yn-26-1	Galena	18.410	15.620	38.560
BTW4	Galena	18.405	15.598	38.462	Yn38-2	Galena	18.280	15.450	38.040
BTW5	Galena	18.374	15.504	38.243	Yn41-2	Galena	18.400	15.550	38.360
BTW5	Sphalerite	18.426	15.684	38.266	Yn42-2	Galena	18.350	15.530	38.290
BTW7	Galena	18.443	15.628	38.516	After Ye et al. (1992)				
BTW8	Galena	18.405	15.552	38.334	J26	Galena	18.196	15.398	38.164
Yn16	Galena	18.267	15.465	38.117	J27	Galena	18.299	15.469	38.135
Yn23	Galena	18.266	15.436	38.032	J28	Galena	18.223	15.425	38.099
Yn25	Galena	18.238	15.404	37.900	J61	Galena	18.161	15.362	38.101
Yn30	Galena	18.321	15.496	38.177	J65	Galena	18.205	15.376	38.007
Yn31	Galena	18.347	15.521	38.281	J66	Galena	18.235	15.401	38.009
Yn38	Galena	18.371	15.540	38.311	J69	Galena	18.286	15.420	38.300
Yn41	Galena	18.289	15.450	37.993	J72	Galena	18.184	15.390	38.182
Yn42	Galena	18.350	15.532	38.281	J27	Sphalerite	18.326	15.489	38.160
Yn45	Galena	18.351	15.516	38.167	J28	Sphalerite	18.285	15.470	38.297
Yn46	Galena	18.310	15.483	38.160	J60	Sphalerite	18.232	15.435	38.106
Yn55	Galena	18.345	15.513	38.204	J61	Sphalerite	18.217	15.374	38.124
Yn59	Galena	18.187	15.390	37.889	J65	Sphalerite	18.400	15.607	38.216
Yn61	Galena	18.324	15.495	38.169	J70	Sphalerite	18.315	15.461	38.176
Yn87	Galena	18.332	15.488	38.145	J27	Pyrite	18.351	15.499	38.168
Yn93	Galena	18.320	15.430	38.230	J29	Pyrite	18.345	15.524	38.283
Yn13-1	Galena	18.312	15.473	38.135	J60	Pyrite	18.402	15.542	38.329
Yn16-1	Galena	18.292	15.498	38.215	J62	Pyrite	18.262	15.468	38.203
Yn16-2	Galena	18.213	15.373	37.927	J69	Pyrite	18.354	15.521	38.214
Yn30-1	Galena	18.374	15.267	38.315	After Zhang (1993)				
Yn30-2	Gelena	18.169	15.351	38.103	82j-2	Galena	18.400	15.612	38.463
Yn31-1	Galena	18.282	15.452	38.040	82j-5	Galena	18.441	15.632	38.660
Yn41-1	Galena	18.401	15.548	38.357	82j-7	Galena	18.285	15.491	38.300
Yn42-1	Galena	18.346	15.526	38.286	82j-9	Galena	18.303	15.501	38.290
Yn46-2	Galena	18.313	15.482	38.157	82j-11	Galena	18.420	15.628	38.536
After Zhou and Zhou (1992)					82j-18	Galena	18.232	15.476	38.174
TY37	Galena	18.283	15.462	38.296	82j-19	Galena	18.283	15.493	38.295
TY38	Galena	18.221	15.422	38.093	82j-26	Galena	18.321	15.450	38.235
TY39	Galena	18.207	15.377	38.007	82j-27	Galena	18.506	15.640	38.557
TY40	Galena	18.214	15.399	38.046	82j-31	Pyrite	18.558	15.617	38.321
TY41	Galena	18.138	15.352	37.921	83j-33	Pyrite	18.600	15.622	38.359
TY42	Galena	18.160	15.361	38.042	82j-35	Galena	18.493	15.619	38.488
TY43	Galena	18.246	15.410	38.225	Lan38	Galena	18.220	15.430	38.090
TY44	Galena	18.288	15.421	38.301	Lan39	Galena	18.210	15.380	38.010
TY45	Galena	18.286	15.452	38.443	Lan40	Galena	18.210	15.400	38.050
TY46	Galena	18.220	15.406	38.155	Lan42	Galena	18.170	15.360	38.040
Ding1	Galena	18.194	15.395	38.112	Lan43	Galena	18.270	15.410	38.230
Ding2	Galena	18.150	15.330	37.961	Lan44	Galena	18.290	15.420	38.300
Ding3	Galena	18.522	15.634	38.480	Lan46	Galena	18.220	15.410	38.160
Ding4	Galena	18.416	15.637	38.639					

5.2. Lead isotopes

Lead isotopic compositions of 94 sulphide (galena, sphalerite, and pyrite) samples from the Jinding Zn–Pb deposit are compiled from previous studies (Bai et al., 1985; Zhou and Zhou, 1992; Ye et al., 1992; Zhang, 1993). The results are shown in Table 3 and Fig. 13.

Ore lead isotopic compositions of the Jinding deposit are characterised by a limited variation in $^{206}Pb/^{204}Pb$, $^{207}Pb/^{204}Pb$, and $^{208}Pb/^{204}Pb$, ranging from 18.1 to 18.6 (mean 18.3), 15.2 to 15.7 (mean 15.2), and 37.8 to 38.8 (mean 38.3), respectively, and show clear linear correlations (Fig. 13). The Pb isotope compositions of the sedimentary rocks are more radiogenetic and form a continuous trend from the ore lead (Fig. 13).

The Jinding ore lead isotopic compositions are significantly different from the crustal lead isotopic compositions in the Lanping–Simao Basin (Table 4,

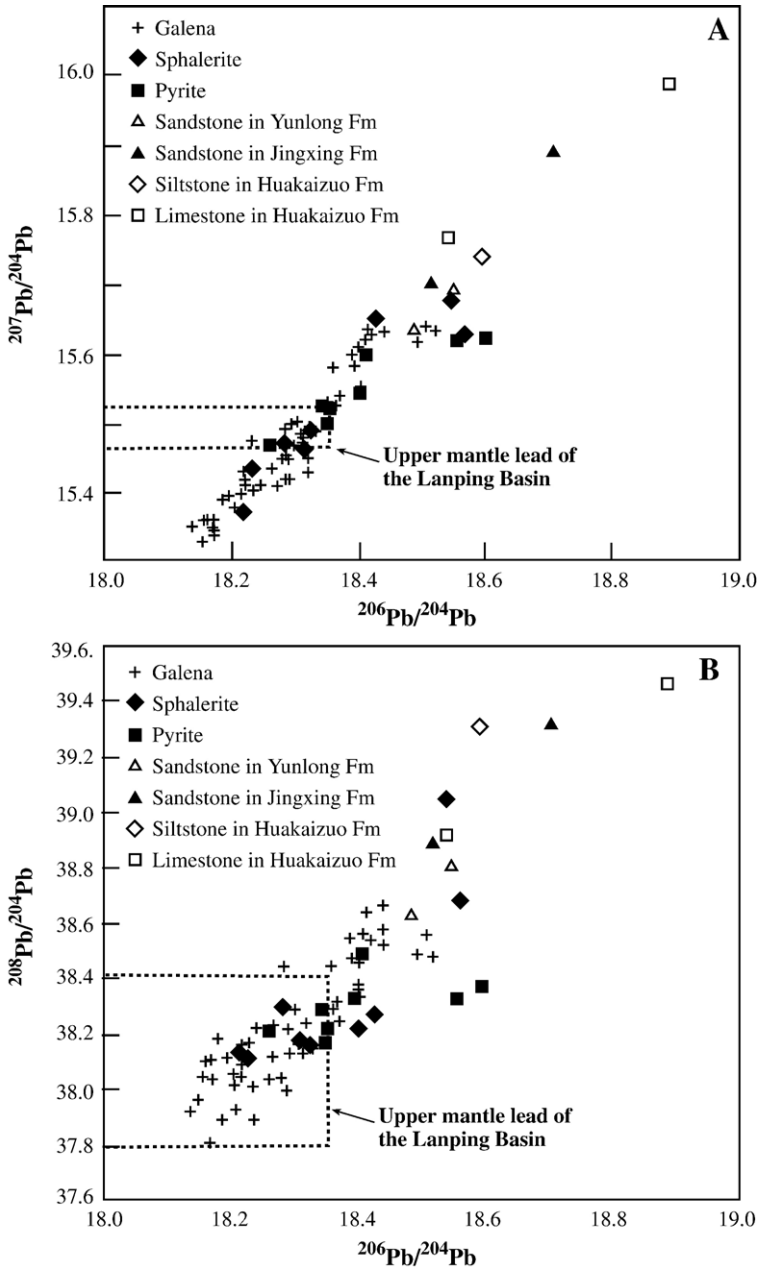

Fig. 13. Plots of $^{206}Pb/^{204}Pb$ vs. $^{207}Pb/^{204}Pb$ and $^{206}Pb/^{204}Pb$ vs. $^{208}Pb/^{204}Pb$ of the Jinding Zn–Pb sulphide ores and some rocks in the Lanping–Simao basin, western Yunnan, China.

Table 4
Rock lead isotopic compositions in the Lanping–Simao Basin, Yunnan, China

Sample no.	Strata	Rocks	$^{206}Pb/^{204}Pb$	$^{207}Pb/^{204}Pb$	$^{208}Pb/^{204}Pb$
JB308	Huakaizuo Formation (Middle Jurassic)	Siltstone	18.592	15.742	39.306
JB439	Yunlong Formation (Paleocene)	Sandstone	18.488	15.636	38.632
JB453-1	Yunlong Formation (Paleocene)	Sandstone	18.549	15.693	38.809
No. 1	Jingxing Formation (Lower Cretaceous)	Sandstone	18.517	15.705	38.888
No. 2	Jingxing Formation (Lower Cretaceous)	Sandstone	18.707	15.891	39.317
No. 3	Sanhedong Formation (Upper Triassic)	Limestone	18.544	15.765	38.914
No. 5	Sanhedong Formation (Upper Triassic)	Limestone	18.888	15.988	39.464
Crustal lead of the Lanping Basin*			18.140–20.289	15.274–16.051	37.878–40.800
Mafic, ultramafic and alkaline rocks in Lanping Basin**			17.877–18.353	15.465–15.523	37.797–38.414

Data is after Zhao (1989b); *after Zhang et al. (2002), Pb isotopic variations of 54 samples including Proterozoic metamorphic rocks and sedimentary (some volcanic) rocks of Cambrian through Tertiary in the Lanping Basin; **after Zhang et al. (2002), Pb isotopic variations of 16 samples including Cenozoic mafic, ultramafic and alkaline rocks along the margin of the Lanping Basin.

Fig. 13), which range from 18.140 to 20.289 in $^{206}Pb/^{204}Pb$, 15.274 to 16.051 in $^{207}Pb/^{204}Pb$, and 37.878 to 40.800 in $^{208}Pb/^{204}Pb$ (Zhao, 1989b; Zhang et al., 2002). On the other hand, the ore lead isotopic compositions partly overlap the upper mantle lead in the Lanping–Simao Basin (Table 4, Fig. 13), as derived from the study of mantle enclaves in Cenozoic magmatic intrusions (Zhang et al., 2002).

The linear change of the ore lead isotopes, their linear correlation with Pb isotopes of the host sedimentary rocks, and the overlap with mantle lead isotopes, suggest a mixing between mantle-derived lead and

Table 5
Sulphur isotopic compositions of sulphide minerals from the Jinding Zn–Pb deposit, western Yunnan, China

Sample no.	Mineral	$\delta^{34}S$(CDT) ‰	Sample no.	Mineral	$\delta^{34}S$(CDT) ‰	Sample no.	Mineral	$\delta^{34}S$(CDT) ‰
After Zhou and Zhou (1992)			After Zhou and Zhou (1992)			After Zhou and Zhou (1992)		
Ty1	Galena	−2.96	Ty53	Pyrite	−13.32	24	Galena	−5.97
Ty2	Marcasite	−21.43	Ty55	Galena	−18.46	25	Galena	−5.36
Ty3	Marcasite	−19.47	Ty57	Galena	−12.04	31	Galena	−3.83
Ty4	Sphalerite	−14.59	Ty58	Sphalerite	−13.00	After Ye et al. (1992)		
Ty5	Pyrite	−19.13	Ty59	Pyrite	−11.55	J26	Pyrite	−13.60
Ty6	Galena	−2.69	Ty60	Galena	−24.91	J26	Sphalerite	−14.62
Ty8	Galena	−14.86	Ty64	Pyrite	−15.21	J26	Galena	−19.90
Ty9	Marcasite	−20.36	Ty65	Pyrite	−16.10	J27	Pyrite	−13.90
Ty10	Pyrite	−3.84	BTW1	Galena	−18.43	J27	Sphalerite	−15.91
Ty11	Galena	−22.68	BTW1	Pyrite	−14.89	J27	Galena	−18.91
Ty12	Marcasite	−12.37	BTW2	Pyrite	−18.82	J28	Sphalerite	−15.15
Ty13	Galena	−2.60	BTW2	Galena	−17.28	J28	Galena	−20.6
Ty14	Sphalerite	−1.71	BTW3	Sphalerite	−15.21	J29	Pyrite	−15.30
Ty15	Galena	−20.50	BTW3	Sphalerite	−15.11	J60	Pyrite	−3.87
Ty15	Marcasite	−13.79	BTW4	Galena	−19.80	J60	Sphalerite	−4.20
Ty16	Galena	−22.68	BTW5	Galena	−9.70	J61	Sphalerite	−3.92
Ty17	Galena	−13.26	BTW5	Sphalerite	−10.58	J61	Galena	−5.63
Ty18	Galena	−20.54	BTW8	Galena	−23.56	J62	Pyrite	−5.68
Ty20	Galena	−12.20	JZK400-1	Pyrite	−15.49	J63	Pyrite	−3.36
Ty21	Galena	−30.43	JZK400-2	Pyrite	−16.80	J65	Pyrite	−3.99
Ty22	Galena	−5.40	JZK402-1	Pyrite	−15.37	J65	Sphalerite	−4.81
Ty23	Galena	−10.50	JZK402-2	Pyrite	−13.48	J65	Galena	−5.92
Ty24	Galena	−6.00	1TS2	Galena	−14.80	J66	Pyrite	−3.45
Ty25	Sphalerite	−7.67	1TG1	Galena	−18.40	J66	Galena	−5.10
Ty26	Pyrite	−13.88	1TG3	Galena	−17.70	J69	Pyrite	−4.01
Ty27	Galena	−16.81	Yn93	Galena	−24.94	J69	Galena	−4.79
Ty29	Galena	−6.60	22	Galena	−5.44	J70	Sphalerite	−7.00
Ty32	Galena	−7.57	23	Galena	−10.50	J72	Galena	−19.3

lead from the host rocks and crustal rocks. The limited variation in ore lead isotopes, compared to the scattered data points for the host rocks and the wide range for crustal lead, suggest that the ore lead was predominantly derived from the mantle.

5.3. Sulphur isotopes

Sulphur isotopic compositions of 83 sulphide samples from the Jinding deposit are compiled from the studies by Zhou and Zhou (1992) and Ye et al. (1992). Results are shown in Table 5 and Fig. 14.

The δ^{34}S(CDT) values of sulphides range from −1.7 to −30.4‰, with a mean of −13.3‰. The ranges of δ^{34}S values of sphalerite, pyrite, galena, and marcasite are −1.7 to −17.3‰ (mean 10.70‰), −3.4 to −19.8‰ (mean −11.3‰), −2.6 to −30.4‰ (mean −13.6‰), and −12.4 to −21.4‰ (mean −17.5‰), respectively. There is a trend of $\delta^{34}S_{sphalerite} > \delta^{34}S_{pyrite} > \delta^{34}S_{galena} > \delta^{34}S_{marcasite}$ (Fig. 14), which indicates an overall non-equilibrium of S-isotopes among sulphides during formation of the Jinding deposit.

The widely variable and negative δ^{34}S values of the Jinding sulphide minerals suggest that organic or bacterial sulphate reduction produced reduced sulphur for the Zn–Pb mineralisation. The widely distributed evaporite sulphates in the Lanping–Simao Basin, whose δ^{34}S values range from 10 to 26‰, especially in the Jinding ore district, are potential sulphur sources for the Zn–Pb mineralisation. The bitumen present in the ores and host rocks testifies the availability of organic material for sulphate reduction.

6. Discussion and conclusions

6.1. Syngenetic versus epigenetic origin and mineralisation age

There have been a number of debates about whether the Jinding deposit is syngenetic (sedimentary exhalative) or epigenetic. The syngenetic hypothesis is largely based on the observations that the orebodies are broadly stratiform and the ores are characterised by fine-grained textures (e.g., Shi et al., 1983; Zhao, 1989a; Qin and Zhu, 1991; Luo and Yang, 1994; Hu et al., 1998). In fact, no exhalative sedimentary rocks have been found in the ore district and surrounding areas. More and more geologists now agree that the Jinding deposit is epigenetic (e.g., Wu and Wu, 1989; Gao, 1989; Hu, 1989; Li and Kyle, 1997; Kyle and Li, 2002). The fact that both the hanging- and footwall of the thrust fault (F_2) are mineralised is the best evidence to support an epigenetic origin, although it has been argued that the host rocks above F_2 are not Cretaceous, but are a continuation of the Palaeocene Yunlong Formation below F_2 (Qin and Zhu, 1991). Other lines of evidence, such as the replacement and open-space filling textures and occurrence of vein-type mineralisation, all point to an epigenetic origin.

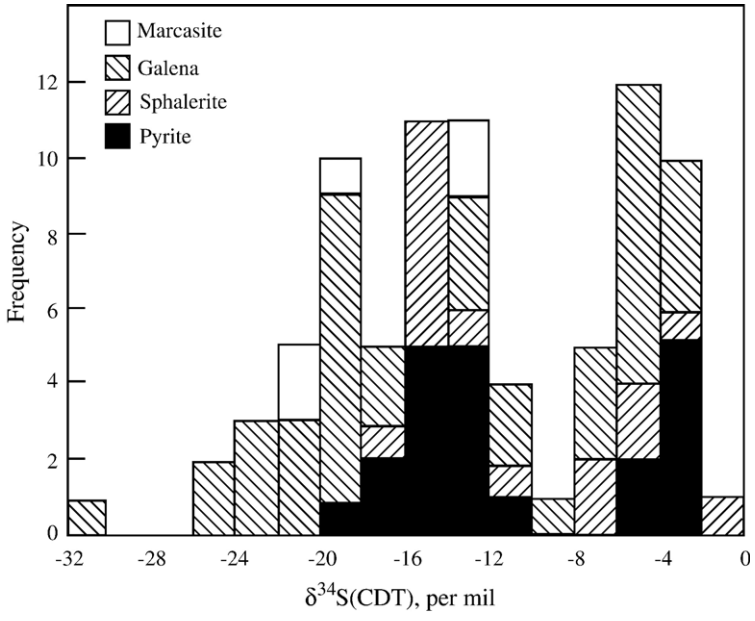

Fig. 14. Histogram of sulphur isotopic composition of sulphide minerals in the Jinding Zn–Pb ores, Yunnan, China.

An epigenetic origin means the age of mineralisation is younger than the youngest host rock, i.e., the Palaeocene Yunlong Formation, which is about 57 Ma. In addition, the mineralisation must have taken place after the emplacement of the nappe on top of the Yunlong Formation; the age of this event is unknown, but it has to be younger than 57 Ma. Furthermore, the distribution of mineralisation around the Jinding dome suggests that the mineralisation is likely coeval or earlier than the formation of the dome structure and could have been folded around the dome. The dome structure is younger than the emplacement of the nappes because both strata above and below the F_2 thrust fault, and the F_2 thrust fault itself are domed. The age of the doming cannot be constrained by geologic evidence directly, but we suspect that the doming may be related to deep-seated magmatic activities, whose age may be similar to some of the exposed alkaline igneous rocks dated between 68 and 23 Ma (Xue et al., 2003). Based on the reasoning above, the mineralisation age at Jinding may be between 57 and 23 Ma.

Direct dating of ore-related minerals from Jinding has been proven difficult, largely due to the fine-grained textures of the ores and the lack of suitable alteration minerals. Xue et al. (2003) used the Re–Os isochron method to date pyrite from the sandstone matrix from the upper ore zone, and obtained an age of 67 Ma. This age is difficult to explain considering the above discussion, and may be related to large errors associated with the small quantity of sample material. However, after taking into account the potential errors, the age of 67 Ma probably indicates that the mineralisation at Jinding may have occurred soon after the deposition of the Yunlong Formation. We consider that the termination of the sedimentation of the Yunlong Formation, the thrusting, and the doming and Zn–Pb mineralisation events successively developed in a short period.

Some other mineral deposits occurring in the Lanping–Simao Basin have been dated with various methods, and may provide a comparison for the Jinding deposit. A 62 Ma age and a 21 Ma age have been obtained (Xue et al., unpublished data) using the ^{39}Ar–^{40}Ar method on fluid inclusions in quartz, and the Re–Os isochron method on pyrite and tetrahedrite, respectively, for the Baiyangping Ag–Co–Cu deposit, 30 km north of the Jinding deposit (Xue et al., 2003). The deposit is hosted in sandstones of the Lower Cretaceous Jingxing Formation (K_1j). The Jinman Cu deposit, hosted in sandstones and siltstones of the Middle Jurassic Huakaizuo Formation (J_2h) and the Lower Cretaceous Jingxing Formation (K_1j), about 30 km west of the Jinding deposit, has been dated to be 58 Ma using the ^{39}Ar–^{40}Ar method on fluid inclusions in quartz (J.J. Liu, personal communication, 2003).

In summary, the age of mineralisation at Jinding has not been dated directly with precision, but is likely to be slightly younger than the end of the sedimentation of the Yunlong Formation (57 Ma). This age falls in the range of significant Himalayan-age alkaline magmatic activities, and is broadly comparable to the mineralisation events elsewhere in the Lanping–Simao Basin.

6.2. Sources of the ore-forming fluids and metals and mechanisms of ore precipitation

Many previous studies (e.g., Zhao, 1989b; Hu, 1989; Gao, 1989; Ye et al., 1992; Zhang, 1993; Luo and Yang, 1994; Hu et al., 1998) considered that the ore-forming fluids and metals of the Jinding deposit were derived from within the Lanping–Simao Basin. However, a number of other studies also indicated that mantle-derived fluids and metals have been involved in the formation of the Jinding deposit (e.g., Yin et al., 1990; Wang and Li, 1991; Xue et al., 2000).

Evidence supporting involvement of mantle-derived fluids and metals in the formation of the Jinding deposit includes the presence of CO_2-rich inclusions (Xue et al., 2002a), which is uncommon in sediment-hosted base metal deposits, the noble gas isotope data indicating significant proportions of mantle-derived gas, and the Pb isotope data indicating dominance of mantle-sourced lead. The presence of alkaline magmatic intrusions that contain mantle-derived enclaves (Lu and Qian, 1999) in the Lanping–Simao Basin and geophysical and remote sensing data indicating magma chamber at shallow depths about 15 to 20 km (Bian, 2000; Xue et al., 2002b) testify the involvement of mantle in the tectonic activities in the region. The active tectonic setting related to the collision between the Indian and Eurasian Plates and the closeness of the deposit to a major deep fault favour the rising of mantle-derived fluids into the Jinding area (Yin et al., 1990; Xue et al., 2002b).

In contrast to Pb isotope data that indicate mantle origin for the metals, the predominance of negative $\delta^{34}S$ values (mean = −13.3‰) of the sulphides indicate that the sulphide was derived from organic or bacterial reduction of sulphates. Evaporites (gypsum, anhydrite, and salts) are widespread in the Meso- and Cenozoic sediments in the Lanping–Simao Basin. The common presence of bitumen in the ores and host rocks at Jinding also indicates that organic matter may have played an important role in sulphate reduction.

The precipitation of sulphide ores at Jinding may be related to the mixing of a mantle-derived, metal-bearing

fluid with a basinal, reduced sulphide-bearing fluid. The mantle-derived fluid is characterised by relatively high temperature and moderate salinity, whereas the reduced sulphide-bearing fluid has relatively low temperature and high salinity. The westward decrease in homogenisation temperature and increase in salinity in the Jinding ore district suggests that the hot, rising fluid moved from the east to the west. The mixing of the two fluids produced fluids of intermediate temperatures and salinities, as shown in the salinity–homogenisation temperature diagram (Fig. 9). The decrease of both temperatures and salinities in the late stage of mineralisation (Fig. 9) may be related to the downward incursion of fresh water with the diminishing of the upward hydrothermal migration.

6.3. Localisation of mineralisation — structural–lithologic trap

The distribution of mineralisation along the F_2 fault and around the Jinding dome indicates that the mineralisation is controlled by structures. Most orebodies are located either on the hanging- or the footwall of F_2, and no mineralisation has been found in other thrust faults parallel to the F_2. The F_2 fault probably acted as both the feeder fault and the ore-hosting structure. The thicknesses of the orebodies tend to increase toward the core of the dome, which may be related to the dilatancy space created by doming that may have facilitated fluid flow toward the core of the dome.

The reason that mineralisation is distributed along the F_2 and not along other thrust faults may be related to the fact that both the hanging- and footwall of F_2 are sandstones or breccia-bearing sandstones, which are permeable, whereas the other thrust faults are developed in rocks of low permeability. The sandstones and breccia-bearing sandstones adjacent to the F_2 are rich in calcareous material as cement or limestone fragments, which can be easily replaced. The combination of the thrust and the dome structures and favourable lithologies may have provided a structural–lithologic trap for the ore-forming material.

6.4. A distinct new type of sediment-hosted Zn–Pb deposit — the Jinding type

The Jinding Zn–Pb deposit may appear to be similar to other sediment-hosted base metal deposits to varying degrees, but it also shows distinct features not shared by others. As discussed above, the stratabound orebodies and fine-grained textures have led some to classify Jinding as a syngenetic deposit and compare it to Sedex-type deposits, but geologic and petrographic evidence indicates it is epigenetic.

There are two major types of sediment-hosted epigenetic base metal deposits, i.e., Mississippi Valley-type (MVT) and sandstone-type (SST). The Jinding deposit shares some similarities with MVTs in mineralogy, open-space filling and replacement textures, and involvement of basinal fluids in mineralisation, but it differs from MVTs in that its host rocks are mainly siliciclastic rocks, whereas the host rocks for MVTs are carbonate rocks. Furthermore, MVT deposits formed from large-scale movement of fluids from within a sedimentary basin (e.g., Qing and Mountjoy, 1994; Garven, 1995; Chi and Savard, 1998), whereas the Jinding deposits formed from mixing of basinal fluids with mantle-derived fluids which were external to the basin.

Perhaps the type of sediment-hosted Zn–Pb deposits that the Jinding deposit resembles most is the SST, both being epigenetic and hosted in sandstones. The origins of SST deposits include formation from shallow groundwater flow (e.g., the Yava deposit, Sangster and Vaillancourt, 1990) and from warm basinal brines (e.g., the Laisvall deposit, Sweden; Rickard et al., 1981). However, in addition to the involvement of mantle-derived fluids, the Jinding deposit differs from the SST deposits in two aspects. First, the SST deposits are characterised by high Pb/Zn ratios, whereas Jinding is a Zn-dominant deposit. Second, the sandstones that host the SST deposits are mature marine quartz-rich sandstones formed in prolonged stable tectonic conditions (Bjørlykke and Sangster, 1981), whereas the ore-hosting sandstones at Jinding are immature continental red beds.

Most importantly, the Jinding Zn–Pb deposit differs from the other types of sediment-hosted base metal deposits in that it was formed in an active tectonic environment, and was structurally controlled. The host rocks of the other types of sediment-hosted base metal deposits are formed in marine conditions, and mostly in relatively stable tectonic environments. The Sedex-type deposits occur in extensional marine basins and formed during the post-rift phase of thermal subsidence (Large, 1988; Sangster, 1990). The Jinding deposit, however, formed in a continental red bed basin that was in a compressional stress regime at the time of mineralisation. Although the migration of ore-forming basinal brines of the MVT and SST deposits may be remotely controlled by orogenies, the mineralisation is not directly controlled by structures.

In summary, although the Jinding deposit shares some similarities with other sediment-hosted base metal

deposits, it is significantly different from the others in terms of tectonic setting, sedimentary facies, structural control, and significant contribution of ore-forming fluids and metals from the mantle. Therefore, Jinding cannot be classified into any of the existing types of sediment-hosted base metal deposits, and represents a new type of deposit. Because Jinding is the first deposit of this type that has been studied in detail, and because of its economic importance, we propose that this new type be called 'Jinding type'.

Acknowledgements

The work is financially supported by the Natural Science Foundation of China (40272050, 40427054), the State Key Basic Research Development Program (2002CB4126007, G1999043201) and the Chinese Post-Doctoral Foundation. We have considerably benefited from discussions in the field with Mr. Luo Junlie. We are also grateful to Professors Mao Jingwen, Qin Gongjiong and Wang Anjian for their help and comments. The detailed and constructive review by C.D. Taylor and an anonymous reviewer on an earlier draft of the paper has significantly improved the quality of the paper. The authors also thanked R. R. Large for reading the manuscript and his constructive comments. The authors are deeply indebted to Khin Zaw and Steven Peters who spent considerable amount of time and efforts to improve the manuscript.

References

Bai, J.F., Wang, C.H., Na, R.X., 1985. Geological characteristics of the Jinding lead–zinc deposit in Yunnan with a special discussion on its genesis. Mineral Deposits 4, 1–9 (in Chinese with English abstract).

Ballentine, C.J., O'Nions, R.K., 1991. The nature of mantle neon contributions to Vienna Basin hydrocarbon reservoirs. Earth and Planetary Science Letters 113, 533–567.

Ballentine, C.J., O'Nions, R.K., Coleman, M., 1996. A magnus opus: helium, neon and argon isotopes in a North Sea oilfield. Geochimica et Cosmochimica Acta 60, 831–849.

Baptiste, P.J., Fouquet, Y., 1996. Abundance and isotopic composition of helium in hydrothermal sulphides from the East Pacific Rise at 13°N. Geochimica et Cosmochimica Acta 60, 87–93.

Bian, Q.T., 2000. A discussion about the relationship between the super large-scale ore deposits and the tectonics of the mantle–crust structure: taking Yunnan as example. In: Tu, G.C. (Ed.), The Super Large-scale Ore Deposits in China. Science Press, Beijing, pp. 545–569 (in Chinese with English abstract).

Bjørlykke, B., Sangster, D.F., 1981. An overview of sandstone lead deposits and their relation to red copper and carbonate-hosted lead–zinc deposits. Economic Geology 75th Anniversary Volume, pp. 178–213.

Chi, G., Savard, M.M., 1998. Basin fluid flow models related to Zn–Pb mineralisation in the southern margin of the Maritime basin, Eastern Canada. Economic Geology 93, 896–910.

Fisher, D.E., 1997. Helium, argon, and xenon in crushed and melted MORB. Geochimica et Cosmochimica Acta 61, 3003–3012.

Gao, G.L., 1989. Review of geological origin about Jinding lead–zinc ore deposit. Earth Science 14, 467–476 (in Chinese with English abstract).

Garven, G., 1995. Continental-scale groundwater flow and geological processes. Annual Review of Earth and Planetary Sciences 23, 89–117.

Hanyu, T., Kaneoka, I., Nagao, K., 1999. Noble gas study of HIMU and EM oceanic island basalts in the Polynesian region. Geochimica et Cosmochimica Acta 63, 1181–1201.

Harrison, D., Bernard, P., Turner, G., 1999. Noble gas behavior and composition in the mantle: constraints from the Iceland Plume. Earth and Planetary Science Letters 171, 199–207.

Hu, M.A., 1989. A preliminary evaluation of the mineralisation and their characteristics on the karst-type lead–zinc deposit by the exemplification of Jinding, Yunnan Province. Earth Science 14, 531–538 (in Chinese with English abstract).

Hu, R.Z., Zhong, H., Bi, X.W., 1998. The helium and argon isotopic geochemistry of Jinding super large-scale lead–zinc deposit. Science in China. Series D 41, 42–48.

Jin, X.C., Wang, Y.Z., Xie, G.L., 2003. Devonian to Triassic successions of the Changning–Menglian Belt, Western Yunnan, China. Acta Geologica Sinca 77, 440–456.

Kennedy, B.M., Hiyagon, H., Reynolds, J.H., 1990. Crustal neon: a striking uniformity. Earth and Planetary Science Letters 98, 277–286.

Khin Zaw Peters, S.G., Gromie, P., Burrett, C., Hou, Z., 2007. Nature diversity of deposit types and metallogenic relations of South China. Ore Geology Reviews 31, 3–47 (this volume). doi:10.1016/j.oregeorev.2005.10.006.

Kyle, J.K., Li, N., 2002. Jinding: a giant Tertiary sandstone-hosted Zn–Pb deposit, Yunnan, China. SEG. Newsletter 50, 8–16.

Large, D., 1988. The evolution of sedimentary basins for massive sulphide mineralisation. In: Frielin, G., Herzig, P. (Eds.), Base Metal Sulphide Deposits. Springer-Verlag, Berlin, pp. 1–11.

Li, N., Kyle, J.K., 1997. Geologic controls of sandstone-hosted Zn–Pb–(Sr) mineralisation, Jinding deposit, Yunnan Province, China —a new environment for sediment-hosted Zn–Pb deposits. In: Pei, R.F. (Ed.), Proceedings, 30th International Geological Congress, vol. 9, pp. 67–82.

Lollar, B.S., O'Nions, R.K., Ballentine, C.J., 1994. Helium and neon isotope systematics in carbon dioxide-rich and hydrocarbon-rich gas reservoirs. Geochimica et Cosmochimica Acta 58, 5277–5290.

Lu, B.X., Qian, X.G., 1999. Petrology research on the deep source inclusions of alkali volcanic rock and alkali-rich porphyry in the Cenozoic Era at western Yunnan. Journal of Yunnan Geology 18, 127–143 (in Chinese with English abstract).

Luo, J.L., Yang, J.Z., 1994. The Tethyan Evolution and the Mineralisation of the Main Metal Deposits in Western Yunnan. Geological Publishing House, Beijing, pp. 149–239 (in Chinese with English abstract).

Mamyrin, B.A., Tolstikhin, I.N. (Eds.), 1984. Helium isotopes in nature. Developments in Geochemistry, vol. 3. Elsevier, Amsterdam. 274 pp.

Norman, D.I., Musgrave, J.A., 1994. N_2–He–Ar compositions in fluid inclusions: indicators of fluid source. Geochimica et Cosmochimica Acta 58, 1119–1132.

Qin, G.J., Zhu, S.Q., 1991. The ore-forming model of the Jinding lead–zinc deposit and prediction. Journal of Yunnan Geology 10, 145–190.

Qing, H., Mountjoy, E.W., 1994. Origin of dissolution vugs, caverns, and breccias in the Middle Devonian Presqu'ile Barrier, Host of Pine Point Mississippi Valley-Type Deposits. Economic Geology 89, 858–876.

Rickard, D.T., Willden, M.Y., Marinder, N.E., Donnelly, T.H., 1981. Studies on the genesis of the Laisvall sandstone lead–zinc deposit, Sweden — a reply. Economic Geology 76, 2052–2060.

Sangster, D.F., 1990. Mississippi Valley-type and sedex lead–zinc deposits: a comparative examination. Transactions - Institution of Mining and Metallurgy. Section B. Applied Earth Science 99, 21–42.

Sangster, D.F., Vaillancourt, P., 1990. Geology of the Yava sandstone-hosted deposit, Cape Breton Island, Nova Scotia, Canada. In: Sangster, A. (Ed.), Mineral Deposit Studies in Nova Scotia, vol. 1. Geological Survey of Canada Paper 90-8, pp. 203–244.

Sarda, P., Staudacher, T., Allègre, C.J., 1988. Neon isotopes in submarine basalt. Earth and Planetary Science Letters 91, 73–88.

Shi, J.X., Yi, F.H., Wen, Q.D., 1983. The rock-ore characteristics and mineralisation of Jinding lead–zinc deposit, Lanping. Journal of Yunnan Geology 2, 179–195 (in Chinese with English abstract).

Staudacher, S., Allègre, C.J., 1982. Terrestrial xenology. Earth and Planetary Science Letters 60, 389–406.

Stuart, F.M., Turner, G., 1992. The abundance and isotopic composition of the noble gases in ancient fluid. Chemical Geology 101, 97–109.

Stuart, F.M., Burnard, P.G., Taylor, R.P., Turner, G., 1995. Resolving mantle and crustal contributions to ancient hydrothermal fluids: He–Ar isotopes in fluid inclusions from Dae Hwa W–Mo mineralisation, South Korea. Geochimica et Cosmochimica Acta 59, 4663–4673.

Swindle, T.D., Grier, J.A., Burkland, M.K., 1995. Noble gas in orthopyroxenite ALH84001: a different kind of martian meteorite with an atmospheric signature. Geochimica et Cosmochimica Acta 59, 793–801.

Third Geological Team, 1984. The Jinding Pb–Zn Deposit. Exploration Report, Lanping County, Yunnan Province. Yunnan Bureau of Geology and Mineral Resources, pp. 101–105 (in Chinese).

Trull, T.W., Kurz, M.D., Jenkins, W.J., 1991. Diffusion of cosmogenic ^{3}He in olivine and quartz: implications for surface exposure dating. Earth and Planetary Science Letters 103, 241–256.

Wang, J.B., Li, C.Y., 1991. REE geochemistry of the Jinding superlarge Pb–Zn deposit. Geochimica 19, 359–365 (in Chinese with English Abstract).

Wu, G.G., Wu, X.D., 1989. A preliminary study on the tectonic evolution and mineralisation regularity of the Jinding lead–zinc deposit, Yunnan province. Earth Science 14, 477–486 (in Chinese with English abstract).

Xue, C.J., Wang, D.H., Chen, Y.C., Yang, J.M., 2000. Helium, argon, and xenon isotopic compositions of ore-forming fluids in Jinding–Baiyangping polymetallic deposits, Yunnan, Southwest China. Acta Geologica Sinica 74, 521–528.

Xue, C.J., Chen, Y.C., Yang, J.M., Wang, D.H., 2002a. The CO_2-rich and hydrocarbon-bearing ore-forming fluid and their metallogenic role in the Lanping Pb–Zn–Ag–Cu ore-field, Northwestern Yunnan, China. Acta Geologica Sinica 76, 244–253 (in Chinese with English abstract).

Xue, C.J., Chen, Y.C., Yang, J.M., Wang, D.H., 2002b. Analysis of ore-forming background and tectonic system of Lanping basin, Western Yunnan Province. Mineral Deposits 21, 36–44 (in Chinese with English abstract).

Xue, C.J., Chen, Y.C., Yang, J.M., Wang, D.H., 2002c. Jinding Pb–Zn deposit: geology and geochemistry. Mineral Deposits 21, 270–277 (in Chinese with English abstract).

Xue, C.J., Chen, Y.C., Wang, D.H., Yang, J.M., Yang, W.G., 2003. Geology and isotopic composition of helium, neon, xenon and metallogenic age of the Jinding and Baiyangping ore deposits, northwest Yunnan, China. Science in China. Series D 46, 789–800.

Xue, C.J., Zeng, R., Lui, S., Wang, D., Yang, J., 2004. Geology, fluid inclusion and isotopic studies of giant Jingding Zn–Pb deposit, western Yunnan, China. In: McPhie, J., McGoldrick, P. (Eds.), Dynamic Earth: Past, Present and Future, 17th Australian Geological Convention, 8–13 February, 2004. Geological Society of Australia Abstracts, vol. 73, p. 142.

Ye, Q.T., Hu, Y.Z., Yang, Y.Q., 1992. Regional Geochemistry Background and the Gold–Silver–Lead–Zinc Mineralisation in Sanjiang Area. Geological Publishing House, Beijing, pp. 21–264 (in Chinese with English abstract).

Yin, H.H., Fan, W.M., Lin, G., 1990. Deep factors on the Lanping–Simao basin evolution and the mantle–crust complex mineralisations. Tectonic and Metallogeny 4, 113–124 (in Chinese with English abstract).

Zhang, Q., 1993. Pb isotopic composition of Jinding super-large Pb–Zn in Yunnan Province and discussion on the sources of lead. Geology and Prospecting 29, 21–28 (in Chinese with English abstract).

Zhang, C.J., Ni, S.J., Teng, Y.G., Peng, X.H., Liu, J.D., 2000. Relationship between Himalayan tectonomagmatic movement and mineralisation in Lanping Basin, Yunnan Province. Journal of Mineralogy and Petrology 20, 35–39 (in Chinese with English abstract).

Zhang, Q., Shao, S.X., Liu, J.J., Liu, Z.H., 2002. Pb isotopic compositions and Pb sources of the polymetallic ore deposits in the large ore cluster of Lanping Basin. Acta Mineralogica Sinica 22, 147–154 (in Chinese with English abstract).

Zhao, X.Y., 1989a. On the genesis of the Jinding lead–zinc ore deposit in Yunnan. Earth Science 14, 523–530 (in Chinese with English abstract).

Zhao, X.Y., 1989b. Stable isotope geochemistry of the Jinding lead–zinc ore deposit, Yunnan. Earth Science 14, 495–501 (in Chinese with English abstract).

Zhou, W.Q., Zhou, Q.L., 1992. A study on the isotopic composition of Pb and S in the Lanping Pb–Zn deposit, Yunnan Province. Geochimica 20, 141–148 (in Chinese with English abstract).